Norwegian University of Science and Technology (NTNU)

Centre for Neural Computation (CNC)

Kavli Institute for Systems Neuroscience

Functional Dissection of Local Medial Entorhinal Cortex Subcircuit

Master's Thesis

Faculty of Medicine, Department of Neuroscience

Supervisors: Sheng-Jia Zhang & Jing Ye

Rine Sørlie Wågan

Trondheim, August 2013

Acknowledgements

The work presented in this thesis was performed at the Kavli Institute for Systems Neuroscience and Centre for Neuronal Computation (CNC) at the Norwegian University of Science and Technology (NTNU), under the supervision of Sheng-Jia Zhang and Jing Ye.

Firstly I would like to thank my supervisors for all help and guidance throughout this project. Thanks to you, the last year has been very interesting and I have learned a lot. Thanks to Jean Wu and Jing Ye for helping me with histology and Igans Cerniauskas for doing the perfusions in my project and helping me whenever I asked. Thanks to my excellent class mates for good friendships, assistance, support and laughs. Special thanks goes to Elise Haferstrom, my "study buddy" for five years and Maria Mørreaunet and Torgeir Wåga for being just as "far from sane" as me as the deadline kept getting closer, and for making me laugh, which made my life not as miserable during this period. At last I would like to thank all of my friends and family for support and encouragements.

Table of Contents

Abstract

The superficial layers of the medial entorhinal cortex (MEC) contain several functionally specialized spatial cell types, such as grid cells, head direction cells, border cells and cells with conjunctive properties. It is currently not known how the firing patterns of these cell populations map onto the architecture of the MEC circuit. Results from recent work suggest that there are two largely non-overlapping neuronal populations within superficial layers of MEC with different projecting targets. One of them target the hippocampus while the other projects extrahippocampally. It has been shown that all funtional MEC cell types project to the hippocampus, and a large part of these cells were grid cells. Based on these observations we wanted to investigate if there is a difference in funtional cell distribution of MEC cells projecting to the contralateral MEC and cells projecting to hippocampus.

Retrogradely transportable recombinant adeno-associated virus expressing Flag-tagged channelrhodopsin-2 (ChR2), was injected in left MEC of 6 rats. This introduced optogenetic control over MEC neurons with direct projections to the contralateral MEC. Combining optogenetic and electrophysiological in vivo recordings, allowed identification of functional cell types with direct projection to the contralateral MEC, as these cells showed minimal response latencies to laser stimulations in the medial entorhinal cortex.

We found border cells, head direction cells, non-spatial cells and interneurons with direct projection to the MEC, but no grid cells. This distribution is in contrasts with the one found to project to the hippocampus, where grid cells are the predominant spatial cell type. More data are required to determine if the sparsity of responsive grid cells reflects limited sampling, or if the contralaterally-projecting cell population has distinct functional properties.

Abbreviations

AAV	Adeno-associated virus
AMPA	α-amino-3-hydroxy-5-methyl-4-isoxazole-propionic acid
BGH	Bovine growth hormone
BSA	Bovine serum albumin
CA	Cornu ammonis
CaMKIIα	α-calcium/calmodulin-dependent protein kinase II
ChR	Channelrhodopsin
ER	Endoplasmic reticulum
EC	Entorhinal cortex
HR	Halorhodopsin
HSV	Herpes-simplex virus
ITR	Inverted terminal repeat
LEC	Lateral entorhinal cortex
LED	Light emitting diode
MEC	Medial entorhinal cortex
NMDA	N-methyl-D-aspartate
PBS	Phosphate buffered saline solution
TRIS	Tris(hydroxymethyl)aminomethane
WPRE	Virus posttranscriptional regulatory element

1. Introduction

In the 1930's Edward Tolman proposed the idea that behavior is guided by map-like representations and that these representations were an internal cognitive phenomenon (1). He studied animal's ability to navigate through mazes and discovered that no explicit reinforcement was needed for the animal to perform well in the maze task. This led him to believe that as the animal explores the environment, they are able to discover relationships between places and events and gradually develop the cognitive map (2). At the time the internal "cognitive map" was only an idea that could not be verified by science, mostly because of the lack of tools necessary to investigate the neuronal mechanisms of behavior, but the rich repertoire of spatial behaviors characteristic for several species have made researchers very keen to identify the neuronal basis for representing external space. Today, over 50 years later, the field of neuroscience has evolved to become a mature discipline and it is currently known that there exists brain systems specialized to let the animal know its own location in space.

The discovery of place cells in 1971 (3), contributed to the characterization of map-like neural representations of the external spatial environment. These cells were found in the hippocampus and fired when the animal was located in a particular place in the field (3). These place fields kept their firing in the hippocampus when all the intahippocampal signals were disrupted, which suggests that the place cells get their input from somewhere else and researchers shifted their focus to the entorhinal cortex only one synapse downstream (4). Since then, several different cell types, that are likely contributors in making the intrinsic spatial map, have been discovered.

In the entorhinal cortex there are a number of different functional cell types that appear to make up the basis of neural representation of the external space. These are called head-direction cells, border cells and grid cells (5). Head-direction cells fire only when the head of the animal is facing a specific direction (6). Border cells fires when the animal is close to edges and corners in the environment (7). The grid cells form a specific triangular firing pattern, when the animal is moving around in an open area, which does not appear to represent any specific properties in the external environment (8).

Ever since the spatial cells, especially the grid cells, were discovered the spatial representation and navigation system has been used as a model to investigate neuronal computation in non-sensory cortical microcircuits. One example is the characteristic crystal-like firing pattern of the grid cells been studied to get insight in the neuronal interactions responsible for pattern formation in the brain. The properties of hippocampal and entorhinal cells, and how they are connected, has been a research topic of large interest the last decade, this in an attempt to establish the mechanisms by which microcircuits in these areas encode, maintain and update representations of location as animal moves through the environment. A lot of new and useful insight has been discovered about the spatial representation and navigation system that tell us something about how the brain works, but there are still a lot we do not know about this intriguing system in the brain.

1.1 Hippocampal region

The hippocampal region is divided into two different cortical stuctures; the hippocampal formation (HF) and the parahippocampal region (PHR). The main difference between these structures is the number of cortical layers and the overall principles of connectivity (9).

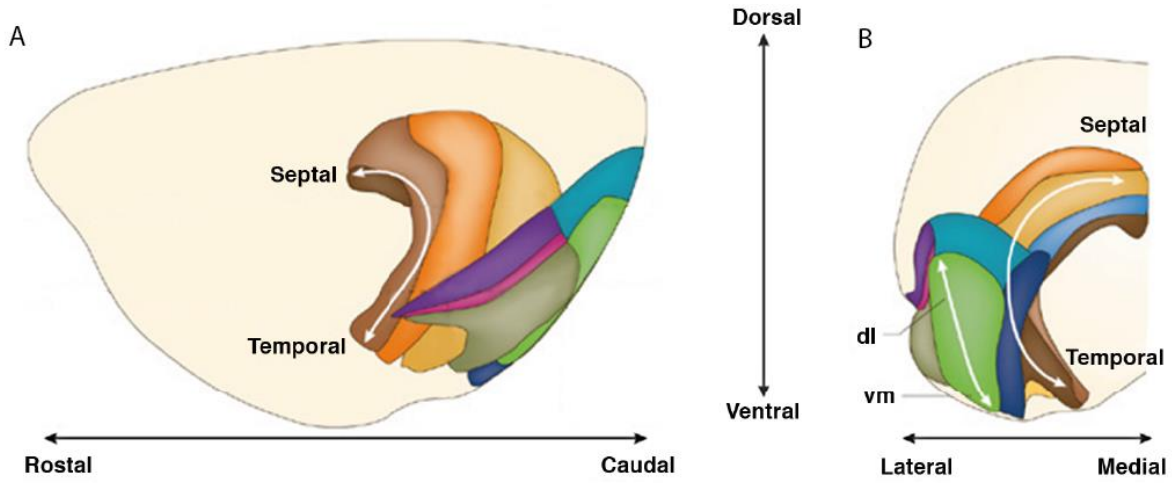

Fig. 1. The hippocampal region represented as a schematic. (A) Lateral view. Septotemporal axis is indicated. Black arrows showing the rostal/caudal and dorsal/ventral axis. (B) Coronal view. Dorsolateral/ventromedial axis indicated. Black arrows showing lateral/medial axis. Colors representing different subregions in the hippocampal region are described in Fig. 2. Illustration taken from (10).

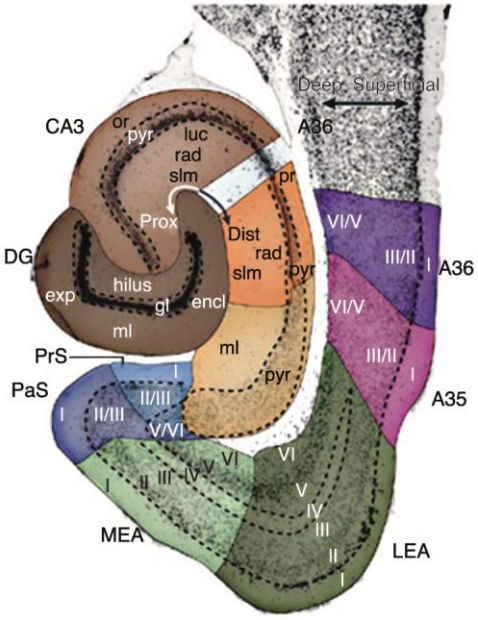

Fig. 2. The hippocampal region represented by a Nissl-stained horizontal cross section. Proximal/distal (prox-dist) axis and deep/superficial axis are shown. Different subregions in hippocampus and parahippocampal region are shown in different colors: dentate gysus (DG, dark brown), CA3 (light brown), CA1 (orange), subiculum (yellow), presubiculum (PrS, light blue), parasubiculum (PaS, dark blue), medial entorhinal cortex (MEA, light green), lateral entorhinal cortex (LEA, dark green), Brodmann areas 35 (A35, pink) and 36 (A36, purple). The Roman numerals indicate cortical layers, the further abbreviations represent: enclosed blade of the DG (encl), exposed blade of the DG (exp), granule cell layer (gl), stratum lucidum (luc), molecular layer (ml), stratum oriens (or), stratum radiatum (rad), stratum lacunosum-moleculare (slm). Illustration taken from (10).

1.1.2 Hippocampal formation

The hippocampal formation (HF), a c-shaped structure situated in the caudal brain consists of the subregions hippocampus proper (consisting of CA3, CA2 and Ca1) the dentate gyrus and the subiculum. The hippocampal formation is formed by a three layered cortex where the deep layer is made up of afferent and efferent fibers and interneurons, the middle layer consists of principal cells and interneurons and the most superficial layer is referred to the as the molecular layer (10).

1.1.3 Parahippocampal region

Adjacent the HF is the parahippocampal region (PHR) bordering the subuculum. It has six layers and consists of the five subregions: the presubiculum, the papasubiculum, the entorhinal cortex (EC), the perirhinal cortex (PER) and the postrhinal cortex (POR) (10).

1.1.4 Entorhinal cortex

The entorhinal cortex is located in the ventroposterior convexity of the rat cerebral hemisphere. It extends ventromedially to border either the parasubiculum medially or the piriform cortex. Rostrally it borders the amygdaloid complex and dorsolaterally it extends to approach the rhinal fissure. The entorhinal cortex ends just ventral to the rhinal fissure at rostral levels and at caudal levels it extends within and slightly above the rhinal fissure.

The entorhinal cortex can be divided into two general areas: the lateral entorhinal cortex (LEC) and medial entorhinal cortex (MEC). The two areas can be differentiated by for example looking at the cells size, distribution of cells and how easy it is to differentiate between cell layers (11). The terminations of the projecting fibers are also slightly different. The fibers from MEC end up in the proximal part of CA1 and the fibers from LEC terminate more distally in the CA1 (9).

The entorhinal cortex contains a substantial system of associational connections. In the data available, it looks like the intraentorhinal fibers are mainly directed in a longitudinal direction and the connections that link mediolateral regions or transverse regions of the entorhinal cortex seem to be few (12,13). The associational connections originate in both deep and superficial layers where projections from layer II and III mainly terminate in the superficial layers and the projections from deep layers terminate in both deep and superficial layers (11).

1.2 The brain's spatial map

1.2.1 Place cells

The hippocampal place cells are pyramidal cells that fire when the animal is located in a specific position in the environment, but not anywhere else. Different place cells fire at different positions, called place fields. Even though the place cells do not show any apparent topographic arrangement in the hippocampus, recordings of a large number of cells in a rat brain show that the activity of these cell ensembles is unique for every location in the environment and therefore it would be possible to reconstruct the accurate position of the rat (14). This could indicate that there is a spatial map of the environment that is being formed by these cell populations (15). This map might be innate, at least so is suggested by the findings showing that place cells are present in rat brains already 15 days after birth, this soon after the rat pups open their eyes (16, 17). These cells are not only dependent on visual cues since they fire both in light and dark, but probably have some other input they depend on (18).

When animals are moved to different environments, different subsets of neurons are recruited in the hippocampus (19), suggesting that the hippocampus contains multiple representations that are associated with every space that the animal experiences. Another feature of the hippocampal place cells is that minor alterations in the same experimental environment, such as sensory or motivational input, change the firing patterns of the cells. This is referred to as remapping (19, 20, 21, 22, 23). When for example the color or the shape of the environment

was changed or when the reward contingencies changed, the place cells showed new place fields and the old ones disappeared or moved. These observations which implied that the hippocampal representation would be very great, lead researchers to think that the computation of the position would not be in the hippocampus. To look for the place where the metrics of the spatial map were computed, entorhinal cortex was an obvious candidate since this area is only one synapse upstream or downstream of the place cells in the hippocampus (24).

1.2.2 Grid cells

In the medial entorhinal cortex there has been discovered another class of position-selective neurons called grid cells (8, 25). When a rat is running in an open-field arena, the grid cells show multiple firing locations that make up a hexagonal pattern over the entire area where the rat has been running. About 50% of the principal cells in layer II are grid cells (6). Grid cells in the same part of the MEC have grid spacing and grid orientation that are similar to each other, but the phase of the grid is non-topographic which means that the firing fields of cells that are near each other in the brain, seem to shift randomly (8). From dorsal to ventral position in the entorhinal cortex there is an approximately linear increase in the spacing of the grid pattern ranging from one field repetition per 30 cm to distances over several meters in the rat (8, 25, 26).

The grids of different cells are offset relative to each other. In this way each place in the environment can be identified from only a few cells' activity as long as they have some variation in spacing. Convergence of inputs from grid cells that got overlapping fields but differ in their spacing can be the origin of individual place field in the hippocampus (27, 28, 29). The grid cells can be seen as a element of a dynamic and constantly updated map showing the animal's position in the environment, this based on the fact that the position of an moving animal can be reconstructed from an assembly of grid cells' activity (25). Across environments the grid map persists in a stereotypic manner, unlike the place cells, this could suggest that the map is applied anywhere, but the particular phase and orientation of the grid can change across environment which could mean that the grid is strongly determined by geometrical features of the environment (30).

1.2.3 Border cells

Border cells are cells that fire only along geometrical borders of the environment available to the animal. Most of the border cells fire only along one side of the border and maintain their

activity when the environment is stretched or when the animal is tested in different rooms and enclosures with different sizes and shape. Suggested by the findings that show that these cells keep firing when the border is so small that the animal can step over it, and when boundaries are made by elevated platform, border cells are active at the presence of a border and not the physical features of a wall (30). Even though the border cells are more sparse than grid and head-direction cells (comprises less than 10% of local principal cell population), their role in spatial representation could still be significant because they are widely distributed in all layers of MEC (15).

1.2.4 Head-direction cells and conjunctive cells

Head-direction cells have also been found in the entorhinal cortex and have properties that likely are involved in spatial mapping. As previously mentioned, these cells will increase their firing rate whenever the head of the animal faces a certain range of directions relative to the surrounding landmarks. The head-direction cells are found in layer III to VI of MEC (6).

Conjunctive cells, which are grid cells modulated by head-directionality have been found in the layers below layer II of the MEC. These cells increase their firing rate when the animal is passing through a grid field and the head turned in a specific direction (6).

All of the functional spatial cell types found in the entorhinal cortex could be part of a metric navigation system where the grid cells could be responsible to map distances, head-direction cells would be able to map directions and the border cells the position relative to boundaries (15).

1.3 Circuits

1.3.1 Hippocampal circuit

A lot of the neocortical information reaching hippocampal formation go through the entorhinal cortex and therefore this structure can be considered the first step in the intrinsic hippocampal circuit. The cells in the superficial layers of entorhinal cortex send information to the dentate gyrus via an axon bundle called the perforant path. This pathway is unidirectional, which means that the projection goes only from entorhinal cortex to the dentate gyrus and not the other way around. The granule cells in the dentate gyrus projects to the pyramid cells of the CA3 in the hippocampus via their axons called the mossy fibers. This pathway is also unidirectional. Likewise are the axons of the pyramid cells in the CA3 called the Schaffer collaterals which forms synapses with cells in the CA1. The cells in the CA1

project unidirectionally to the subiculum and the entorhinal cortex. The cells in the subiculum send their axons to the presubiculum and the parasubiculum, but the most prominent projection goes to the entorhinal cortex. Both the connections from CA1 and subiculum end up in the deep layers of entorhinal cortex and close the hippocampal processing loop which begins in the superficial layers of entorhinal cortex. (11)

1.3.2 Entorhinal microcircuit

The perirhinal cortex and postrhinal cotex are responsible for major cortical inputs to the entorhinal cortex. The LEC gets its input preferably from perirhinal cortex and the postrhinal cortex projects to the MEC. The fact that the majority of axons terminating in the LEC and MEC have their origin in two different areas, has led to the consumption that the MEC pathway transmit spatial information and the LEC transmit non-spatial information. The entorhinal cortex provides reciprocal connections to the peri- and postrhinal cortices (31).

As previously mentioned the entorhinal cortex consists of six cell layers and the laminar organization of LEC and MEC do not differ (32). Layer I consists of two different types of GABAergic interneurons defined by their morphology: horizontal and multipolar neurons. These cells are embedded in a dense plexus of axons which originates from several afferent areas. Multipolar cells are often positive for calretinin and projects to principal cells in layer II and III. Horizontal cells express multiple other markers and have their axons entering the white matter noncollaterizing. Both cells types are almost spineless (32).

In layer II of MEC there are mostly stellate cells (33) and in LEC there are fan cells (34). In the deeper part of layer II there are pyramidal-like cells. All of the different cell types found in layer II of EC have some different electrophysiological properties, but they all show hyperpolarization-activated current (Ih) which is not found in layer III neurons (34). The principal cells in MEC receive excitatory inputs from the presubiculum on their layer I dendrites and the inhibitory signals synapse on unidentified GABAergic interneurons inn the same layer (35). A number of the layer II cells' efferents go toward the angular bundle and continues to its main targets in the dentate gyrus and CA2/CA3. This is the first component of the perforant path. Although the main targets for these axons are in the hippocampus, the axons give off thin collaterals in layer I and II for intrinsic connections (33).

Layer III of EC has mainly pyramidal neurons. Axons from the presubiculum provide strong excitatory and inhibitory inputs in MEC (35) and excitatory inputs from CA1 and subiculum target principal cells throughout the EC (36). Inputs from the postrhinal cortex synapse onto principals cells in MEC (37). The pyramidal cells of layer III's main axons project via the angular bundle to the subiculum and CA1. This is the second component of the perforant path (32).

Layer IV is referred to as lamina dissecans and contains only a few neurons that can be characterized either as layer III or layer V cells in addition to a number of interneurons. The neurons in this layer are likely innervated by axons from the medial septum, pre and parasubiculum and monoaminergic brainstem inputs. These also distribute across all layers of EC (9).

In layer V there are large pyramidal cells located just below the lamina dissecans. Their apical dendrites go through the superficial layers and might reach the pial surface and the basal dendrites spreads mainly in the deep layers. In the deeper part of layer V there are smaller cells which generally are horizontal pyramidal, multipolar or fusiform cells and they tend to have dendritic trees confined to layers V and VI, but some of the apical dendrites may cross the lamina dissecans into layer III. The basal dendrites receive input from CA1 and the subiculum (36). MEC layer V pyramidal cells' basal dendrites will likely also get some inputs from retrosplenial cortex and medial prefrontal cortex (38). The apical dendrites will get their input from presubiculum (39). All principal cells in layer V send a main axon into the white matter (40) projecting to multiple cortical and subcortical targets (9).

Layer VI contains mostly of multipolar neurons. They got spiny dendrites which extend within layer VI, occasionally reaching the angular bundle and layer V (32). The inputs to layer VI are likely the same as in layer V. The axons join the underlying white matter, projecting to thalamic midline nuclei (9).

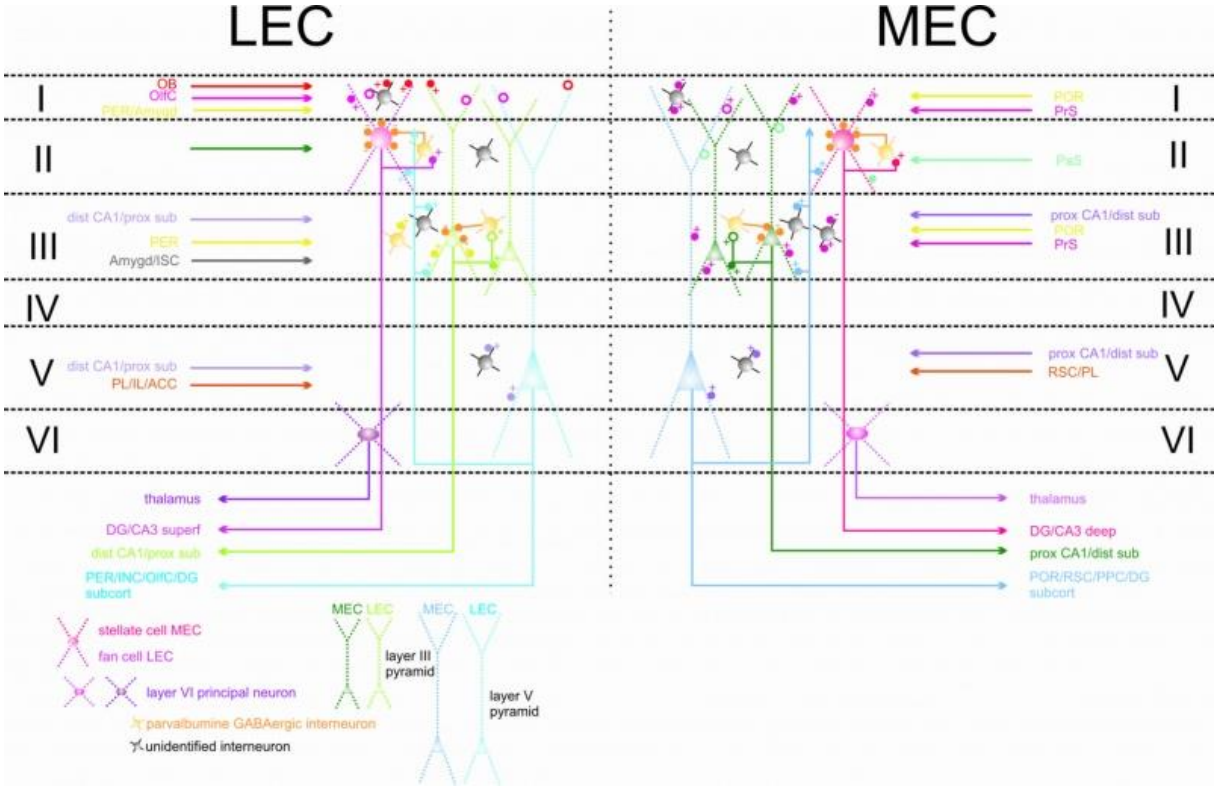

Fig. 3. Main neuron types and connections of lateral entorhinal cortex (LEC) and medial entorhinal cortex (MEC) represented as a schematic. Inputs and output are color coded and represented in their main layer (indicated by the Roman numerals), of origin and termination. Different cell types and their main dendritic and axonal connections are coded with a unique color. The big red cell formed as a cross in layer II represents stellate cell in MEC and fan cell in LEC. The smaller pink and purple cross-like cell in layer VI represents layer VI principal cell. The green cells formed as a triangle in layer III represent layer III pyramidal cells (light green in LEC and dark green in MEC). The blue triangle-shaped cells in layer V represent layer V pyramidal cells (light blue in LEC and dark blue in MEC). The small dark yellow colored cells in layer II and III represent parvalbumine-positive GABAergic interneuron and the small black cells in layer I, II, III and V represent unidentified interneurons. The filled small circles are representing synaptic contacts. Open circles represents inferred, but not established synaptic contacts. Illustration taken from (41).

1.3.3 Functional cell type projections from entorhinal cortex to hippocampus

Even though multiple findings done over the last 10 years indicates that there is some connection between the spatial cells found in the entorhinal cortex and the place cells of the hippocampus, there have not been determined what functional cell types is responsible for this connection. Several discoveries suggest that the cells of MEC do have some effect on how the place cells are formed. For example do the areas CA1 and CA3 receive inputs from layer II and III of the MEC which both contains grid cells, head-direction cells and border cells (8, 31). When lesions where done to the intrahippocampal inputs in CA3 the CA1 place cells persisted (4), and when the lesions was done so that the inputs from MEC layer III to CA1

were disrupted the activity of the place cells was impaired (26). These findings suggest that the cells of entorhinal cortex probably are important for the place cell activity, but it does not tell us which functional cell types project to the hippocampus. A recently published study may provide some answers to this question.

In a recently published study optogenetics along with electrophysiological recording equipment were used to identify the functional cell types in the MEC projecting to the hippocampus (42). A retrograde transporting virus containing channelrhodopsin-2, a light activated molecule, was injected into the hippocampus and inserted tetrodes (tool to record electrophysiological cell activity) and an optical fiber (tool to provide laser light into the brain), into the MEC of living rats. When shining laser light onto the MEC cells while recording their electrophysiological activity, identification of the cells that were responsive to the laser by selecting cells with minimal response latency to the flashing laser light, were enabled. These cells were considered likely to project to the hippocampus. To identify the functional cell type of the responsive cell, the firing pattern recorded while the rat was running in a square box, were evaluated. Responsive grid cells, head-direction cells and border cells, but also irregular spatial cells and non-spatial cells, were identified. The grid cells were found to be a large contributor to the population with entorhinal-hippocampal projection (42).

1.3.4 Contralateral entorhinal projections

There are relatively strong commissural connections arising from all portions of the entorhinal cortex. They terminate predominantly in layers I and II of the homotopic area (13, 14).

In a previously study, findings suggest that it could be two different cell populations within the layer II of entorhinal cortex with different projection targets (43). Reelin and calbindin were used to label two major, equally abundant, non-overlapping cell groups: one immunoreactive to reelin and the other to calbindin. When the retrograde tracer biotinylated dextrane (BDA) were injectd into the ipsilateral dentate gyrus mostly of the cells BDA-labeled was reelin positive cells. This suggests that that only reelin positive cells project via the perforant path to the hippocampus. The calbindin positive cells did not project to the dentate gurus. After, injection in the hippocampal commissure/fimbria-fornix region was made with the retrograde tracer fluorogold, and the majority of fluorogold-labeled cells were

calbindin positive cells in the layer II MEC this could indicate that the calbindin neurons project extra-hippocampally.

Based on earlier findings that show an entorhino-entorhinal connection travelling through the dorsal hippocampal commissure (44), further led to testing if calbinding-expressing cells in the MEC layer II send their axons to the contralateral entorhinal cortex (43). To do so, a unilateral injection of retrograde tracers into the MEC, were made. The most of the labeled cells in the contralateral MEC were calbindin positive, which suggest that calbindin positive cells projects contralaterally to entorhinal cortex.

In the very same paper (43) it is suggested that cholecystoknin and cannabinoid type 1 receptor expressing basket cells (CCKBCs), which are the major regulator of principal cells in the hippocampal networks, do only target calbindin expressing neurons. This means that these particular GABAercic cells only synapses on cells that project outside hippocampus. The CCKBC avoid the reelin positive cells that project to the dentate gyrus which suggests that the GABAergic targets principal neurons depending on their long-distance axonal targets (43).

1.4 Computational models

Ever since the discovery of place cells (3), researchers have tried to find out how the brain is able to make an internal spatial map based on the external environment. Early it was suggested that the place cells would not give enough information to be the only component in the brain's navigational system. (14). The discovery of grid cells in the entorhinal cortex (25) gave rise to multiple computational models of the grid field formation and how the grid cells are involved in generating the place fields in the hippocampus.

1.4.1 Path integration

As previously mentioned, the spatial representation of the entorhinal cortex in contrast to the hippocampal map, will maintain the intrinsic firing structure of the cell assemblies across environments. This suggests that the entorhinal network consists of a single map that can be used universally across all environments (45). The map has a rigid structure and it does not depend on particular landmarks so the firing positions might be integrated in the grid cells from speed and direction signals without referring to the external environment. Studies have shown that even though the speed and the direction of the animal changed the grid fields stayed in the same positions, even in darkness the firing fields persisted. This suggests that

self-motion information probably is responsible for keeping track of the animal's position in the environment (8, 38). This is referred to as path- integration and it may provide a metric component to the spatial map (45).

1.4.2 From grid cells to place cells

Considering that the majority of principal cells in layers II and III of MEC project to the hippocampus the place cells are likely to receive most of their cortical input from grid cells (9). It is not currently known exactly how place cells convert the multiple firing fields characteristic for grid cells into a single place field, but there are at least two sets of possible mechanisms:

A linear combination of signals from grid cells with different grid spacing could generate place fields (30). This will also create a periodic pattern, with a peak where most of the contributing cells are in phase. The spacing of this periodic pattern would be so large that only one field would appear in normal experimental settings. Only a combination of 10-50 grid cells with different grid spacing and orientation, but the same spatial phase are needed to create single fields in models (30).

Another mechanism is based on competitive Hebbian learning processes. The place cells receive input from grid cells with variable spacing, orientation and spatial phase (46). The single place field is generated by the resulting distribution of activity peaks. Experimental findings support only parts of this theory since the place fields develop also when NMDA-receptors, necessary for long-term potentiating learning mechanisms are blocked (47). Competitive learning mechanism may be responsible for formation of new cell assemblies when the animals are introduced to a novel environment (48).

1.4.3 Oscillatory-interference grid cell model

When the grid cell was discovered, the oscillatory-inference model was used to describe how the grid cells work (49). It was suggested that the grid patterns emerge from velocity-dependent beat frequencies in the membrane potential which are a consequence of interference between multiple theta oscillators with different frequencies (50). In the single cell model, the soma (cell body) was thought to be the baseline oscillator and the dendrites functioned as the other oscillators that interact with the baseline oscillator. Each dendritic oscillator's frequency is determined by how fast the animal is moving in a specific direction. If the preferred directions of the inputs reaching the different dendrites are 60 degrees relative

to each other, this will lead to the characteristic triangular grid pattern when the oscillation of the dendrites is combined with the soma (51).

1.4.4 Attractor network model

The network of neurons that has self-stabilizing activity state is called an attractor network. The term is increasingly common amongst neuroscientist, but stems from the mathematics of dynamical systems. It describes a system of interacting units (in this case neurons), which, when given a fixed input, will evolve over time to a stable state (52).This model can also explain how spatial representation can emerge.

The attractor model hypothesize that the grid pattern are a result of "packets" of localized excitation on a flat energy landscape provided by recurrent connections. When a certain level of global inhibition is added to this network, random patterns of activity will give rise to an organized "bump of activity. This bump is centered on mutually connected cells which may have the same set of firing vertices (27, 28). The activity bump can move between grid cells with different vertices as the animal moves to one place to another in a two-dimensional environment. This model is based on path integration mechanism where it is thought that changes in the direction and speed modulates the connectivity between the cells (53).

1.4.5 Modules

Recent findings suggest that the grid populations are discretized into functionally independent subpopulations. As previously mentioned the grid map's scale increases topographically from dorsal to ventral MEC, but it seems that the grid scale do not increase gradually, but rather in a step-like matter. More than one grid orientation was found in the same animal and the discontinuities in grid orientation coincide with discontinuities in grid scale. When changes was made in geometry of environment, cell populations with different grid properties responded independently, which indicate that the grid modules can be anchored separately to external cues (54).

1.5 Optogenetics

Optogenetics are techniques that have emerged recently in the field of neuroscience and the interest for the benefits this technique offers has made it a rapid evolving field of technology. The technique combines optics, genetics and bioengineering and makes it possible to control the activity of specific cell types by either stimulating or inhibit opsins which are light-sensitive membrane proteins (55, 55, 57, 58). Compared to classical electrical or multicomponent manipulation techniques, optical control by microbial opsins has several

advantages. This technique can for instance by genetic targeting stimulate or inhibit specific cell types in the brain. Electrical stimulation could not do this and will interfere with all cells present, even though they have different genetic or anatomical entity. Because of this, an optogenetic approach will often be preferable over electrical stimulation when studying how individual elements contribute to brain circuits (59).

1.5.1 The evolution of optogenetics

In 1979 Francis Crick pointed out that there would be beneficial for the field of neuroscience if there was a way to control only one type of cells and leave the others unaltered. Since electrodes could not target specific cells and drugs would work too slowly, an idea that the use of light could be used as a control tool was presented, but at the time there was no such method available (60).

Even though the idea of using light as a control tool was published in 1979, there were some groundbreaking discoveries done earlier that would have a great impact on the development of optogenetics. In 1971 it was discovered that bacteriorhodopsin functioned as an ion-pump that gets activated by visible light-photons (61). Later, one of the first successive attempts to control cell activity using bacteriorhodopsin was made by activating abdominal ganglion cells in the sea slug Aplysia (62). Ever since that discovery researchers have tried to improve the technique that offers optical control of neuronal activity.

In 1983, fluoroscent dye and light was used to initiate action potentials in neurons (63). The technique of optogenetics developed fast, and in 1994 researchers successfully inhibited cells in Drosofolia by combining laser and chromofore (64). Later, the microbial opsins halorhodopsin (65) and channelrhodopsin (55), were discovered.

1.5.2 Opsins

Throughout history, organisms have evolved different kinds of mechanisms to help them harvest light because of survival functions. One of these mechanisms is preformed by a 7-transmembrane opsin gene family. Because of their simple structure, meaning that light-sensing and effector domains both are encoded in one single gene, and fast kinetics, microbial opsins are tools that is often used in optogenetics.

To enable reaction to light, each opsin protein needs retinal, a vitamin A-related organic cofactor that functions like an antenna for photons. This opsin-retinal complex is called

rhodopsin. The retinal molecule is fixed in the binding pocket of the 7-transmembrane helices, and here it is covalently attached to a conserved lysine residue of helix 7 and forms a protonated retinal Schiff base. When the retinal absorbs a photon, it isomerizes, and this will lead to a triggering of structural changes which again will lead to channel opening, ion transport or signaling transducer proteins will start to interact (66).

By choosing different kinds of opsins you could manipulate cell activity by either activating or inhibiting them. There are opsins that are light-activatable cation-conducting channels which will depolarize the membrane potential of the cells and might lead to an action potential (for example channelrhodopsins). There are also opsins that function by hyperpolarizing the membrane potentials via light-activatable chloride and proton pumps (for example halorhodopsin and bacteriorhodopsin). Activating these opsins could lead to inhibiting an action potential. There are also engineered rhodopsin-G protein-coupled receptors (GPCR) chimeras that are able to control intracellular G-protein-coupled signaling cascades (for example OptoXRs). They are made by replacing the intracellular domain of vertebrate rhodopsin with the intracellular loops from GPCRs (66).

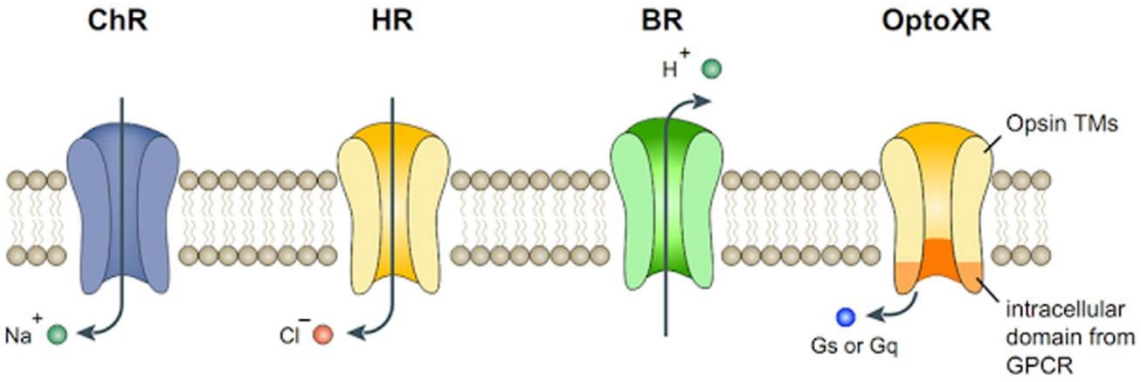

Fig. 4. Types of opsins represented by a schematic. Channelrhodopsins (ChR), are light-activated cation channels which conducts sodium (Na^+). Halorhodopsins (HR) and bacteriorhodopsins (BR) are light-activated chloride (Cl^-) and proton pumps (H^+, hydron). OptoXRs enable light-activated control of intracellular G-protein-coupled signaling cascades. Illustration taken from (66).

There are two types of opsin genes, one is microbial opsin (type I) and the other is animal opsin (type II) (67). Type I opsins control different functions such as energy storage, phototaxis, development and retinal biosynthesis. They are found in algae, fungi and prokaryotes (68). Type I opsins encode proteins that use retinal in the all-trans configuration which isomerizes to the 13-cis configuration when a photon is absorbed. The activated retinal

molecule in type I rhodopsin will not dissociate from its opsin protein, but maintain a covalent bond to its protein partner while it reverts to its all-trans state (69). This reaction occurs rapidly and this is why when used as optogenetic tools, it allows microbial rhodopsin to modulate neuronal activity at high frequencies (70, 71, 72, 73).

Type II opsins are found in higher eukaryotes and are mainly responsible for vision, but can also play a role in circadian rhythm and pigment regulation (74, 75). This type of opsin is classified as a G-protein-coupled receptor and it uses all the 11-cis isomer of retinal for photon absorption. When the light hits the opsin, the 11-cis retinal isomerizes into the all-trans configuration and initiates protein-protein interaction instead of ion flux. This will trigger the visual photo-transduction second messenger cascade. In contrast to opsin type I, the retinal in opsin II, will after isomerization dissociate from its opsin partner into the all-trans configuration and due to this, a new 11-cis retinal have to be recruited. Because of chromophore turn over reactions and requirement for interaction with downstream biochemical signal transduction partners, the effect opsin type II has on cellular changes will be much slower than the kinetics in opsin type I.

Because opsins have combined sensor and effector in a monocomponent system, they do not need exogenous genetic or chemical substitution which makes them suitable for in vivo experiments. Also the fact that light of moderate intensity does not interfere with neuronal function and that opsin latency when illuminated is very short, is an advantage of using the optogenetic approach because it allows cell type-specific control with millisecond time scale and it is fully reversible (59).

1.5.3 Channelrhodopsins

One type of the single-component microbial transmembrane ion conductance regulators are the channelrhodopsins. There are two types of these as well: channelrhodopsn1 (ChR1) and channelrhodopsin2 (ChR2). ChR1, a light-gated ion channel, was found in *Chlamydomonas reinhardtii* which is a green unicellular alga. First it was thought to be only proton-selective (55), but later it became clear that it has a broader cation conductance, including Na+ and K+ (76, 77). ChR2 was later discovered in the same organism and this opsin also conducts protons, but compared to ChR1 the conductance for Na+ and K+ is twice as great (56, 77). The ChRs can be inserted into the plasma membrane of the neurons and make changes in the membrane potential by illumination of blue light around 480nm (70, 73). The expression of

ChR2 was found to be enough in mammalian neurons that it was possible to achieve precisely timed light-driven action potentials (70). ChR2s have fast onset kinetics with time constants on the order of milliseconds and are therefore able to transduce high frequencies of millisecond-lasting light flashes into reliably evoked action potentials (66).

Even though optogenetics and the use of channelrhodopsins are new developed techniques they have already been applied successfully in a number of studies. For instance is channelrhodopsin used in brain slice preparations, where either a DPSS laser is used to focus light trough an optical fiber positioned in a micromanipulator, or LEDs are utilized. The ChR2 must be expressed in excitable cells and activating them in the tissue with the use of laser light can be compared to using electrical stimulating electrodes, but here you can select specific cell types by genetic targeting (78). An example of optogenetics used in vitero is the experiment, where they used channelrhodopsin-2 in thalamocortical slices from mice brains to explore the role of thalamocortical and intracortical synaptic cooperatively in driving up-states in spontaneous slow oscillations. They found that optogenetics improved the study of thalamocortical pathways in slices, because the responses in thalamus resemble those observed in vivo. The result indicated that more synaptic cooperatively (caused by either thalamocortical or intracortical fast AMPA-receptor excitation), lead to more robust inhibition of up-states (79).

Another approach where channerhodopsin has been used, is in vivo recording. The components that are surgically implanted in the animal have to be small for minimal impact on the behaving animal. It is also possible to thread a fresh optical fiber down an implanted guide cannula for each experiment. By using this method it is also possible to infuse drugs into the brain structure prior to optical activation (78). An example where optogenetics were used in vivo is a study where mice models were used to explore temporal lobe epilepsy. The findings suggest that either inhibition of excitatory principal cells (HR) or activation of a subpopulation of GABAergic cells (ChR2), stops seizures rapidly upon light application. These results show that temporal seizures can be detected and stopped by modulating specific cell population in a spatially restricted manner (80).

1.6 Delivering tools

In addition to efficient transcription, expression and safety, optogenetics requires specific in vivo targeting of the optogenetic tool. Major categories in targeting and delivering strategies are viral promoter targeting, projection targeting, transgenic targeting, and spatiotemporal targeting.

1.6.1 Viral delivering

Viral vectors are versatile tools that are being used to deliver genetic constructs into neurons. This tool offers multiple advantages for optogenetics that includes fast and versatile implementation and high potency copy number linked to high gene copy number, and capability for multiplexing genetic and anatomical specificity. Viral vectors are for these reasons the most used delivering tool at the moment (81).

The two most used types are lentiviral vectors (LV) (82) and adeno-associated viral vectors (AVV) (83), and both of them have successfully been used to introduce opsins into mouse, rat, and primate brain (84). The expression levels have been high over long time periods for these vectors and there has not been reported any adverse effects. LV could easily be produced with traditional laboratory equipment using standard tissue cultures (72, 84), but this would be difficult in the case of AAV that can be produced in individual laboratories using kits such as Virapur or through core virus production facilities. AVV-based expression vectors have some properties that often make it preferred over LVs. For example does AVV vector have low immunogenicity that makes the transduced tissue volume lager compared to LV. Also the LV is permanently integrated into the genome of targeted cells, which can lead to undesired disruption of host genes, while the AVV vector is mainly maintained outside of the chromosome (84).

There are different types of AVV vectors, one of them is the recombinant AAV2 (rAAV2) vectors. There are also various serotypes packaging systems within this category, for example rAAV2/1, rAAV2/2 and rAAV2/5. There are some differences across the different serotypes when it comes to expressing when introduced to the nervous system. rAAV2/1 and rAAV2/5 have higher transduction frequencies in all regions injected in the rat's CNS than rAAV2/2. Also rAAV2/1 and rAAV2/5 was observed in particular areas of the CNS after retrograde transport (85).

Although the viral delivery method has multiple advantages and is frequently used by scientists, its major disadvantage is the limited packaging capacity. AVV can accommodate transgene constructs up to 5 kilobases (kb) and LV up to 10 kb. Because of this AVV and LV are only used to deliver small promoters from approximately 2 kb-5kb; microbial opsin gene plus a fluorescent tag can take up to 2 kb of sequence length. Since some cell-type-specific promoters have much longer regulatory elements, using viral delivery methods will limit the expression specificity. Another disadvantage by using this particular method is when targeting small brain nuclei the spatial precision of stereotaxic injection is limited. Also when large regions of brain tissue are targeted multiple injections are required for achieving efficient expression (84).

Microbial opsin products can move down dendrites or axons and create light-sensitive projections often with help from molecular engineering, such as the addition of cellular trafficking motifs (86). In this case the transduction of cell bodies in one brain area, and recruiting cells by delivering light to the axonal projection in another, will make it possible to define cell populations by virtue of their wiring. This does not require any genetic information about downstream target (87, 88).

Another approach for targeting specific neural projection is to use trans-synaptic viral vectors or proteins with anterograde or retrograde-transporting properties (89, 90, 91). When these are engineered with recombinases they can activate gene expression in subpopulations of neurons with cell-type and circuit-specificity. For example, wheat germ agglutin or tetanus toxin fragment C that contains Cre, can be expressed in one brain region while the recombinase will be transported either presynaptic or post-synaptic to a neuron in another brain region (86). Also retrograde- and anteriograde- transporting viral vectors such as rabies virus, herpes simplex virus (HSV) family viruses, vesicular stomatitis virus, pseudotyped LVs or certain serotypes of AVVs can be used for delivering recombinases or transgene cassettes trans-synaptically to neurons (86, 92, 93). With either Cre-dependent transgenic mice or viral vectors combined with conditional expression system, it would be possible to allow circuit-specific gene expression in a variety of animal models (66).

1.6.2 Transgenic animal targeting

One of the challenges of using viral system is the limited packaging capacity, this can be overcome by using another strategy; transgenic animals. Cell-type-specific opsin expression can be achieved by using local promoter-enhancer regions in mouse transgenic lines that directly expresses opsin genes. The development of several transgenic mouse lines that express channelrhodopsin and/or halorhodopsin under the pan-neuronal Thy-1 promoter has been successful (94, 95). One disadvantage with this particular method compared to viral delivery, is that it is very time consuming to generate and breed transgenic animal lines. Also, to avoid undesirable gene interruptions, each transgenic animal line needs to be carefully characterized because of the untargeted nature of the transgene insertion.

1.6.3 Spatiotemporal targeting

Spatiotemporal targeting is a method where cells can be targeted by virtue of their birthdate or proliferation status or location at moment in time. It is possible to target specific layers of the neocortex using this approach (87, 96, 97, 98). In utero electroporation (IUE) con be used to target opsins to particular layers of the cortex by incorporating the DNA into neurons generated during a specific embryonic stage (96, 97).

1.7 Electrophysiological recordings

Ever since Galvani discovered that the nervous system was linked to electrical activity for more than 200 years ago (99), investigators throughout history have tried to build instruments capable of measuring the electrical activity. Today modern electrophysiological tools are sensitive and got high temporal resolution, which makes it possible for researchers to study a wide variety of nervous system function, from properties of single ion channels to the activity of neuronal networks consisting of hundreds of cells (100).

Electrodes made of either metal, glass or silicone are being used to record electrical signals which are a consequence of ion fluxes across the neuronal membranes. Electrophysiological recordings make it possible to understand how the neurons work and communicate with each other at a high signal-to-noise ratio (100). In the vicinity of their somata action potentials produce large transmembrane potentials. By placing a conductor near the neuron it is possible to measure these voltage differences (101). Because neurons of the same cell class will have similar action potential, the electrode tip has to be moved closer to the cell body to be able to identify one single neuron from the extracellulary recorded spikes. To make it easier to

distinguish the activity from one specific neuron from the activity of the rest, wire tetrodes consisting of four spaced wires can be used. There are numerous advantages by using wire tetrodes instead of sharp-tip single electrodes, for example larger yield of units, low-impedance recording tips and mechanical stability. With this tool there is no need to place the recording tip in the immediate vicinity of the neuron and therefore it is possible to do long-term recordings in behaving animals (102).

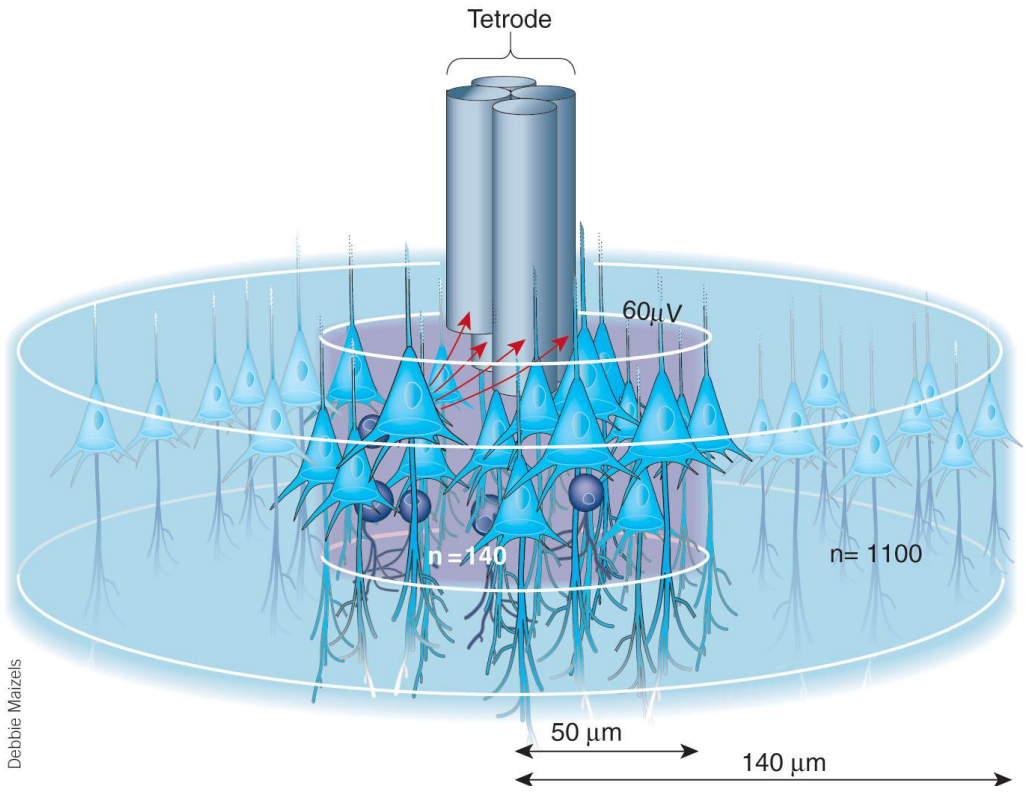

Fig. 5. A tetrode inserted in neural tissue represented by a schematic. Pyramidal cells are represented by blue triangles and the red arrows indicated the distance between the visible electrode tips and a single pyramidal cell. The inner cylinder has a radius of 50 µm and contains 140 neurons (n=140) with a spike amplitude of 60 µV. The amplitude of cells within this cylinder can be separated with available clustering methods. The outer cylinder had a radius of 140 µm and contains 1100 neurons (n=1100) the amplitude of cells within this cylinder can also be detected by the tetrode. Illustration taken from (102).

2 Aim

Insights into the underlying computations in the hippocampus and entorhinal cortex can be translated to other areas in the brain. Understanding the algorithms for spatial navigation can contribute to more knowledge about brain function and can also change the way we are treating multiple diseases. For this reason more research on these particular brain areas is important because it may contribute better treatment and improved life quality of patients suffering from different neurological diseases.

The hippocampal-entorhinal spatial system is also closely related to memory. Not only are we able to remember multiple navigational routes important in our lives, but based on our experiences in the past we can often remember clear details of events and items that we associate with specific places. The same areas in the brain that are involved in guiding navigation; the hippocampus and entorhinal cortex are the same that support declarative memories (103). It has been speculated that the same networks and algorithms support both mental (memory) and physical (navigation) forms of travel (104). It would be beneficial to understand the networks and algorithms of the hippocampus and the entorhinal cortex because we might learn how the brain is able to form and retrieve memories and maybe in the future help people suffering from memory loss etc.

The hippocampal and parahippocampal region is an interconnected and functionally complex system and subregions within this region contributes to different functions within a larger system. Investigating and understanding the anatomical wiring of a network can contribute to gain insights into the function of a system.

The aim of our project is to reveal what functional MEC cell types projects to the contralateral entorhinal cortex and it is based on recent findings (43) suggesting that there are two different non-overlapping cell populations positive for two different markers in the layer II of the MEC that have different projection targets. The findings suggest that one of the populations projects to the dentate gyrus and the other projects outside the hippocampus for instance the contralateral entorhinal cortex. Several functionally defined cell populations have been found in the entorhinal cortex, for example, grid cells, head-direction cells and border cells. Understanding the wiring of these cell populations and their projection patterns are important in order to understand the information flow within the system. All of the functional cell types

mentioned above, plus irregular spatial cells, non-spatial cells and interneurons have been reported to project to the hippocampus, but grid cells appeared to be the major contributor to this projection (42). We ask if the cells projecting contralaterally from MEC to MEC differed in functional cell type distribution compared to the cells projecting to hippocampus. The aim of this project is therefore to identify the functional MEC cell types that projects contralaterally to the entorhinal cortex.

3 Methods

Note

Procedures for virus preparation and surgery were performed by Sheng-Jia Zhang, procedures for histology were performed by Juan Wu and Jing Ye and perfusions were performed by Ignas Cerniauskas. These procedures are described briefly in the method section since they are essential parts in this project and will create a better overview.

3.1 AAV plasmid constructs

The light driven cation channel channelrhodopsin- 2 was chosen to induce neuronal activity in this experiment. For delivering the opsin's genetic constructs to the neurons in the entorhinal cortex a recombinant adeno-associated viral vector (rAVV) flanked by serotype-2 inverted terminal repeats (ITRs), was used. All viral constructs were generated by a polymerase chain reaction (PCR)-based amplification and cloning method. In addition to the ChR2 the rAAV2/1 vectors contained a woodchuck hepatitis virus posttranscriptional regulatory element (WPRE) and a bovine growth hormone (BGH) polyadenylation signal for enhancing transgene transcription and expression. For transcriptional regulations all viral expression cassettes were regulated by a calcium calmodulin-dependent protein kinase II a (CaMKIIa) promoter, which drive transduction of rAAV2/1 in both principal cells and interneurons. AFLAG-tag was placed at the C terminus of all opsin genes between a 20 amino acid trafficking signal DYKDHDGDYKDHDIDYKDDDDK and an endoplasmic reticulum (ER) exporting motif FCYENEV, both of them derived from Kir2.1 potassium channel. All of this was done to enhance the trafficking of opsins.

3.2 rAAV preparation

The rAAV2/1 was prepared by co-transfection of human embryonic kidney cell line HEK293 and an adenoviral helper plasmid pHelper. Normal growth medium replaced the DNA/CaCl2 mixture after 12 h. The transfected cells were collected and subjected to three freeze/thaw cycles after 60 h in culture. Then a purification of the clear supernatant was carried out using heparin affinity columns (HiTrap Heparin HP, GE Healthcare, Uppsala, Sweden). After that, the purified rAAV2/1 was concentrated in an Amicon Ultra-4 centrifugal filter 100K device (Millipore, Billerica MA, USA). By using StepOnePlus Real- Time PCR Systems (Applied Biosystems, Foster City, CA, USA) and TaqMan Universal Master Mix, viral titres of all prepared rAAV2/1 were determined. At last the viruses were diluted and matched to 1.0 x 1012 viral genomic particles/ml by 1 x PBS.

3.3 Subjects

6 male Long-Evans rats (2-3 months old, 400-500 g at surgery) were used to extract data from neuronal activity recording. When at rest (not during recording), the rats stayed in a transparent Plexiglas cage (45 x 30 x 35 cm), one by one in a temperature and humidity controlled room approximately 10 m from the recording room. The recordings were executed during the dark phase of a 12h dark/ 12h light cycle which was kept in the vivarium. The rats were kept at 85-90% free-feeding body weight and water was available ad libitum. 18-24 h before training or recording session the rats were food deprived. All experimental protocols are in accordance with Forsøksdyrutvalget (**http://www.mattilsynet.no/fdu/**) regulations.

3.4 Surgery

rAAV2/1 (1.0×10^{12} viral genomic particles/ml) was injected in the left MEC Injection volumes were 0.5-1 µl. During the same surgical procedure animals were implanted with 125 µm wide optical fibers in hippocampus and tetrode-optical fiber assembly (optrode) in both left and right MEC for 4 rats and only in right MEC in 2 rats. Each tetrode bundle consisted of four tetrodes cut flat at the same level. Tetrodes in MEC were implanted 0.1-0.5 mm in front of the transverse sinus, 4.5-4.7 mm lateral to the midline, 1.6-1.8 mm below dura, and oriented at an 8-20 degree angle in the anterior direction in the sagittal plane. Optical fiber tip was located 500 µm above the tetrode tips in MEC; what is more, 26G cannula was implanted near the optrode in MEC for drug infusion. The tetrodes were made of 17 µm polyimide-coated platinum-iridium (9:1) wire with platinum-plated electrode tips.

3.5 Training and recording

After the surgery the rats were given 3-7 days to recover before the training started. The rats were trained to run in a 1 x 1 x 0.5 m square box with black walls and black floor. To make it dark during recording, curtains surrounded the box, and to avoid signal noise, the box was electrically grounded. A white cue card (21 x 30 cm) was fixed on one of the box's walls to polarize it. To motivate the rats to run in the box, covering the whole space available, crushed chocolate cereal was thrown scattering the box. Behavioral training continued for about a week until the running coverage was acceptable.

There were two typed of data collecting sessions: one running session as described above and one laser session. During the laser session the rat was placed on a towel to run freely in a flower pot on a pedestal. When the data collecting session started the rat was place in the flower pot and connected to the recording equipment (dacqUSB Recording System";Axona,

UK) via AC-coupled unity gain operational amplifiers near the head of the rat. Allowing the rat to move freely in the pot and in the box a counterbalanced cable was used. The tetrodes were moved in steps of 50 μm per day to go deeper into the brain. This procedure was carried out until single neurons could be extracted from the data, then recording session followed. After the recordings were done and no changes in the units were shown, the tetrodes were lowered yet again.

3.6 Spike sorting, position data and rate maps

By using cluster-cutting software (Tetrode Interface (Tint), Axona, UK), spike sorting was performed. This program is specialized for the analysis of spatially-specific neural activity. It generates scatterplots by pairwise comparisons of the 4 electrodes of a tetrode. The clustering of the scatterplots was done manually by hand drawn polygons using two of the parameters the software offers: peak-through amplitude and voltage at time t.

The rat's position was based on tracking one of the LEDs on the head stage.

3.7 Laser stimulation sessions

To identify ChR2 expressing cells laser stimulation session was carried out. An optical fiber (Ø125μm) was coupled to the optical cannula mounted on the animal's head stage while the rat was moving around on the towel in the flower to provide light delivery. Laser light of 473 nm (473 nm Blue DPSS laser (T3); Shanghai Laser & Optics Century, P. R. China) was used for the 2 min. stimulation given at a frequency of 1 Hz. The light pulses lasted for 3.5 ms and the light power at the fiber tip was about 25 mW. If there were cells present in the recorded data a 2 min laser stimulation was given in both right and left MEC before the rat was decoupled from the laser setup and put in the square enclosure to run for 15 min to provide data for cell type identification.

If a responsive cell was found some laser tests was executed. First a normal session of 2 min 1Hz and laser power of 25 mW was done, then sessions with laser power of 5mW, 10mW, 15mW and 20mW all lasting for 2 min and had a pulse frequency of 1 Hz followed. After that, a 2 min session of 5 Hz stimulation was done. At last a 20Hz stimulation session lasting for 30 seconds. For the two lasts session the light pulses came in trains every 5 seconds.

3.8 Perfusion

After some days of turning with no new cell activity and the electrode signal seemed to get lower, lowering of the tetrodes was stopped and the tetrode position remained the same until the perfusion. Food restriction for the rats was also stopped and food was available ad libitum. The day of the perfusion started with weighing the rat to decide the proper amount of

pentobarbital. Then the rat was put in a transparent box (16 cm x 20 cm x 20 cm) along with a paper towel with a few drops of isoflurane. This made the rat unconscious after a few minutes and then the rat received an overdose of 100 mg/ml pentobarbital solution (3ml for a 600 g rat). The pentobarbital was injected intraperitoneally in the abdominal region with a 25G needle (Sterican®; Braun Melsungen, Germany). To check the level of anesthesia toe pinch reflexes was tested and when the rat was in full surgical anesthesia, it was fixed to the perfusion bath by taping the rat's limbs. To expose the rat's heart the chest area was cut open and a 21G needle with running 0.9% saline solution was inserted into the left ventricle. The heart was still beating at the time, and to let the blood run out, a small cut was made in the right atrium. The saline solution was running for about 10-15 min until all of the blood was washed out, then the running saline was replaced with running 4 % formaldehyde solution (pH 7.4) for about 10-15 min. After that the rat's head was cut off and placed in a glass of 4% formaldehyde solution and left for about 1 hour. At last the tetrodes was turned all the way up and the brain was extracted from the caudal part of the skull by removing the skull bones. When the brain was extracted it was kept in a glass of 4 % formaldehyde solution.

3.9 Histology and immunohistochemistry

The brains were stored in the formaldehyde filled glass in the refrigerator for 2 days before it was cut into sections. The non-important parts (hindbrain and olfactory bulb) of the brain were cut off and the two hemispheres was separated by cutting along the longitudinal cerebral fissure using a scalpel. Then one of the hemispheres was mounted onto the microtome holder using mounting medium (Neg -50; Richard-Allan Scientific, USA) and sprayed with pulverized dry ice (101 Cold Spray; Taerosol, Finland). The brain was then frozen for 20-30 min at -21°C and then cut (Microm HM505; Midwest Lab Equipment, USA). The sections were 30 μm thick and made in the sagittal plane. Every second section around the trace area was mounted directly to a 1 % gelatin covered glass slide and the rest of the sections were collected into a 6-well plate which contained 1 x PBS solution.

The sections on the glass slides were stained using Nissl (Cresyl violet) staining. First the sections were soaked in mQ H2O and then dipped 10 times up and down in glass containers with 70 % ethanol, then 80% ethanol and 90 % ethanol and at last three times in containers with 100% ethanol. After the sections was placed in a container of clearing agent 100 % xylene for 2 min, they were rehydrated (3 x 100%, 90% 80%, 70% ethanol) and soaked in a fixing solution (70% ethanol, 0.00% acetic acid) for 5 min. Then the sections were rinsed in

water and left in a container with Cresyl violet solution (0.001% Cresyl violet in mQ H2O). Excess color was washed away with running water and then the sections were dehydrated yet again (70%, 80%, 90%, 3x 100% ethanol) and put in the xylene container for 10 min.

The sections that were collected into the 6-well plate were used for immunostaining. They were washed in 1% Triton solution in 1 x PBS three times for 10 min. Then they were stored over night in blocking buffer (0.1 Triton X-100, 1% BSA, 5% NGS in 1 x PBS) on a shaker at 4°C. The first antibody, 2 µl rabbit polyclonal FLAG, was mixed with 2 ml dilution buffer (0.1 Triton X-100, 1% BSA, 1% NGS in 1 x PBS). FLAG was used to estimate the location of neurons expressing ChR2. The sections were left on the shaker for 2-3 days at 4°C. Next the sections were washed for 2 x 15 min and 2 x 30 min in PBST (0.1% Tween-20 in 1 x PBS). Then the second antibody (4 µl goat anti-mouse antibody conjugated with Cy3 cyanine dye (1 mg/ml)) was added along with 2 ml dilution buffer. Cy3 dye has an emission maximum at 570 nm giving red color to stained sections and its conjugated antibody binds FLAG primary antibody. This was left on the shaker at room temperature for 2 h. After the sections were washed again with PBST (2 x 15 min, 2 x 30 min), they were mounted on gelatin covered glass slides and left to dry over night. The sections were then soaked in Hoechst stain for 2 min in room temperature and washed 1 x PBS for 2 x 30 s and 1 min in mQ H2O. At last a cover glass was put on the glass slides using Eukitt® mounting medium.

4 Results

4.1 Electrophysiological recordings

Tetrode-optical fiber assembles were implanted in MEC of 6 male Long-Evans rats to enable in vivo recordings of electrophysiological activity of MEC neurons. Tetrodes were used instead of stereotrode or single electrode because it allows isolation of single neurons' action potentials from electrical activity of neuronal ensembles. The amplitude of the recorded action potential is a function of distance between the neuron and the electrode and makes the isolation of single neurons possible by triangulation of distances. A cluster-cutting software was used to isolate units (single cell activity). The program visualized the recorded neuronal activity by generating electrode-pair scatterplots. Recorded action potentials were plotted in two dimensions according to their distance to two selected electrodes. Single units were separated manually by hand drawn polygons. Peak-to-through amplitude and amplitude at user-defined time were the two parameters used. Only the clearly separated clusters were counted as cells (Fig. 6).

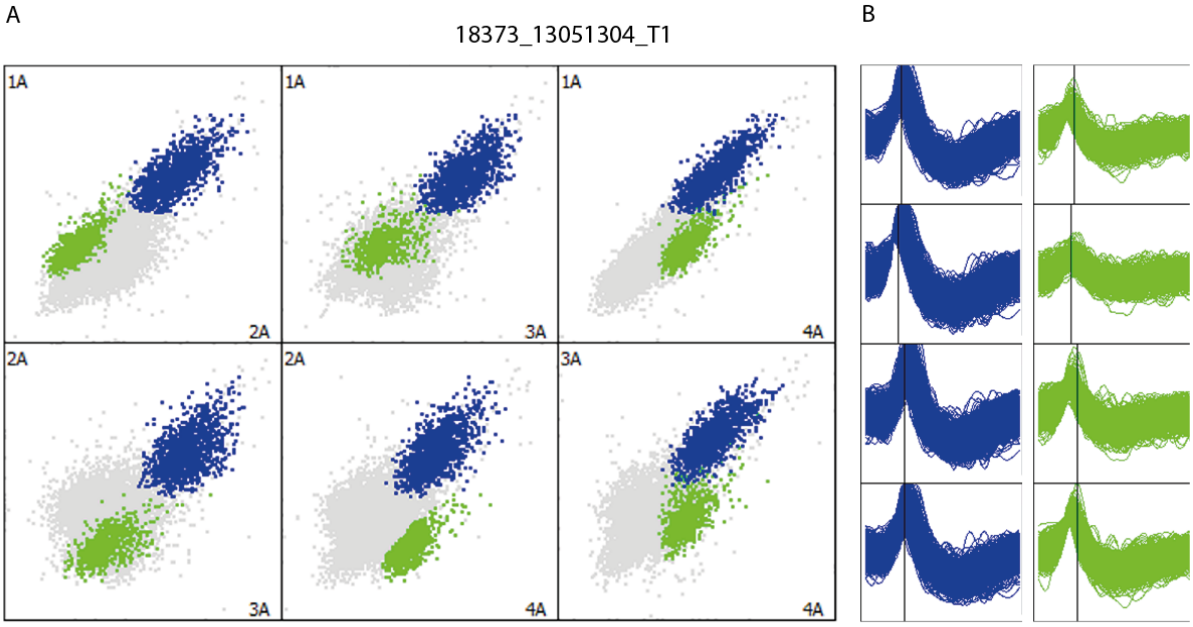

Fig. 6. Isolating single units in cluster-cutting program. (A) Electrode-pair scatterplots showing generated by 10 min of recorded neuronal activity in MEC. The numbers on top of the image indicate the rat number (18273) the date of the recording plus the number of the recording session (130513 – 13. 05. 13, 04 – the forth recording session of the day) and the tetrode number (T1). The grey dots in the scatterplot represent recorded signal and is plotted accorded to the distance to the four electrodes of the tetrode (1A - 4A). Two single units were separated from the rest and clustered into two clusters (blue and green). (B) Recorded action potentials. The blue wave curve corresponds to the blue cluster in (A) and the same goes for the green. Each of the four rectangles shows the recorded action potential of one single electrode.

The recording system (dacqUSB Recording System";Axona, UK) is sensitive and able to detect low frequency electrical activity generated by several cells simultaneously. The use of tetrodes enables separations of single neurons' electrical activity when using a cluster cutting software. Even when tetrodes detect activity from multiple cells simultaneously, it is possible to isolate single units (electrical activity from a single neuron) (Fig. 7.).

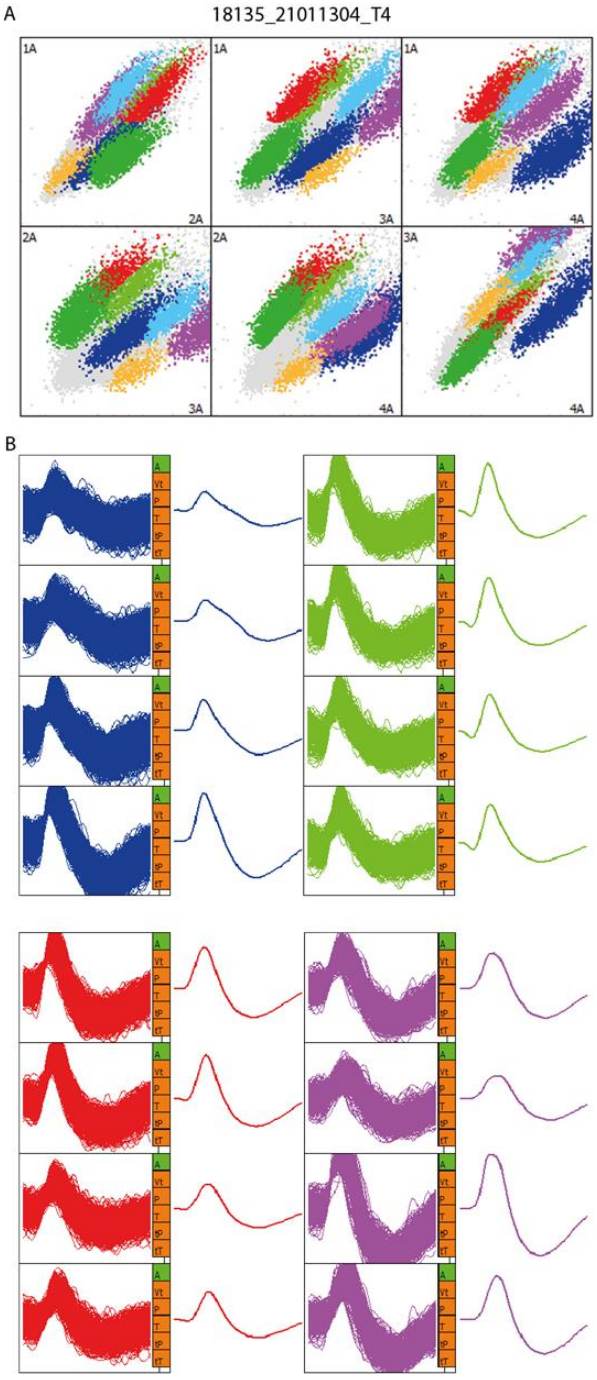

Fig. 7. Multiple clusters within one tetrode. Electrode-pair scatterplots showing generated by 10 min of recorded neuronal activity in MEC. (A) The grey dots in the scatterplot represent recorded signal and is plotted accorded to the distance to the four electrodes of the tetrode (1A - 4A). Seven single units were separated from the rest and clustered into seven clusters, each with different colors (blue, light green, red, purple, light blue, dark green and yellow). (B) Recorded action potentials. The blue wave curve corresponds to the blue cluster in (A) and the same goes for the green, red and purple. Each of the four rectangles shows the recorded action potential of one single electrode. Please note that even though this tetrode recorded multiple units representing cells, all the clusters was clearly separated making the clustering easy.

Optrode was lowered in steps of 50 µm until neuronal activity was detected. Recording session followed, where the rats ran freely in a square enclosure (1 x 1 m) for 10-15 min. Action potentials, along with positional data and tracking of the animal's head-direction, were

recorded and later used to identify functional MEC cell types. After the data were collected at the particular depth of the optrode, and the recorded activity seemed stable, the optrode was lowered until new neuronal activity was detected. The total number of MEC cells recorded was 271. Transcardially perfusion of rats was executed after recordings were finished. The rat brains were cut in sagittal section and stained with Nissl staining to determine final tetrode position. Nissl stained sections shows tetrodes were located in superficial layers of MEC in all 6 rats (Fig. 8).

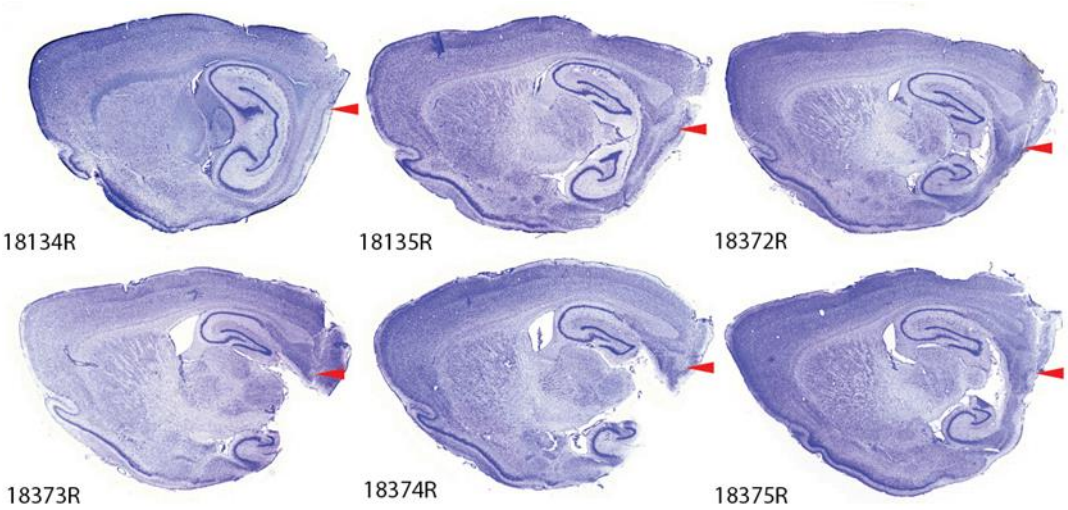

Fig. 8. Nissl-stained sagital brain sections. The red arrow shows the position where the recording tetrode was at its deepest position. The sections is from all of the 6 rats used in the experiment (numbers shows the rat number), and from the right hemisphere (the R shows that the section is from the right hemisphere).

4.2 Determining the Functional Identity of MEC Neurons

To determine the functional cell type recorded path map, rate map, autocorrelogram and head-directional polar, firing rate and waveform of recorded action potentials map was used. Path map shows the rat's trajectory with spike locations marked. Rate map showing the cell's firing distribution. Autocorrelogram made from the rate map showing cross-correlations with itself. A cell was categorized as grid cell if it showed clear triangular firing pattern evident from the rate map. Cells categorized as border cells when it showed a clear firing field along the wall of the box. Another criterion was that it had to show a new firing field along an inserted wall during wall session recording. Cells categorized as head-direction cells when polar firing rate map, showing firing rate as a function of the rat's head direction with peak rate indicated, had a clear preferred direction. Irregular spatial cells had to show some spatial

modulated firing activity, evident in the rate map, but clearly not qualify the criteria set for grid cells and border cells. Cells that did not show any apparent spatial modulation were either categorized as non-spatial principal cells or inter neurons. Differentiation of these two cell types was based on the results from a previous published paper, showing that interneurons have a narrower wave-form than principal cells and that their firing frequencies are higher (Fig. 12).

271 cells were recorded 228 cells were counted as putative principal cells and 33 as putative interneurons. Of the total number of putative principal cells, 72 cells were classified as grid cells (Fig.9), 8 as border cells (Fig. 10), 51 as head-direction cells (Fig.11), 3 as irregular spatial cells and 105 as non-spatial cells.

4.2.1 Grid cells

72 cells were categorized as grid cells. There were cells with multiple small grid patterns, showing multiple small firing fields with small spacing in the rate map (Fig. 9A) and grid cells with bigger grid patterns, showing fewer, but larger firing fields with bigger spacing the rate map (Fig. 9B). 4 of the 72 grid cells recorded had some head-directionality and were considered to be conjunctive grid x head-direction cells (Fig. 9C).

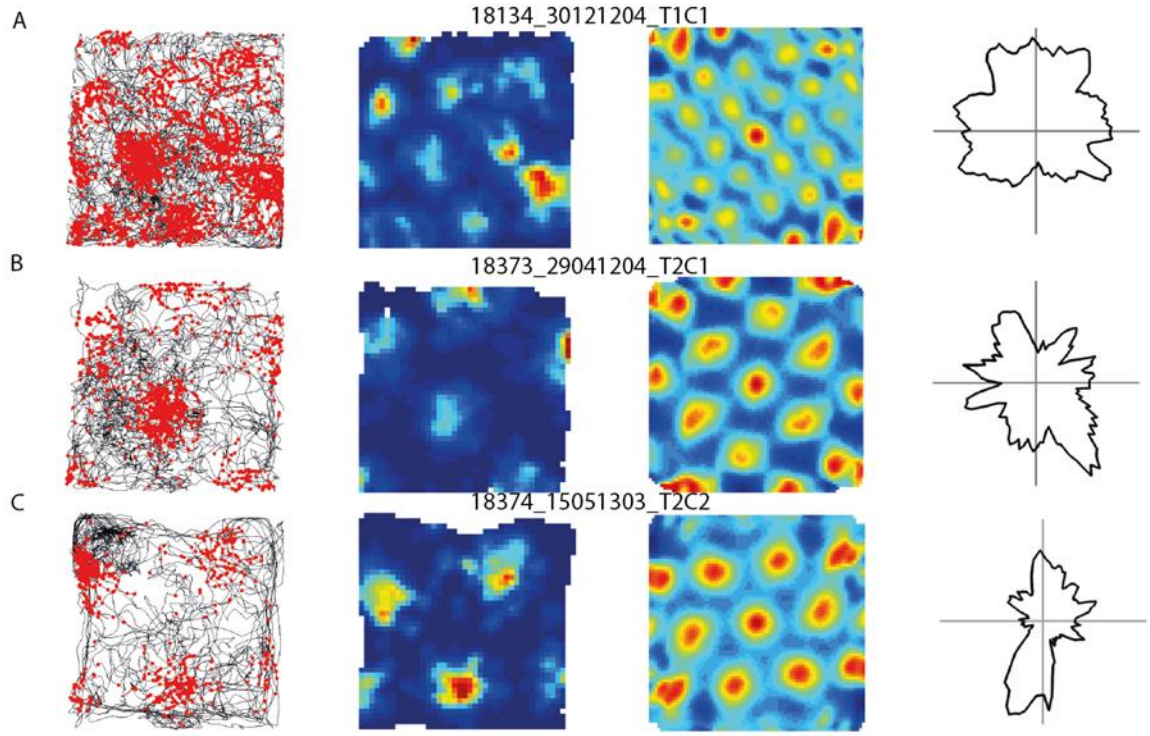

Fig. 9. Examples of grid cells recorded in the MEC of rats running in a square enclosure. (A) From left to right: the rats running trajectory (black line) with spike locations (red dots); a color-coded rate map showing the same cell's firing distribution where the color is scaled from blue (silent) to red (peak rate); a autocorrelogram extracted from the firing rate map with color coded correlation values (blue: low correlation, red: high correlation); a polar map showing firing rate as a function of the rat's head direction with peak rate indicated. The figure arrangement in (A) is the same for (B) and (C). Please note that all (A), (B) and (C) have multiple firing fields shown in the rate map and six-fold rotational symmetry of the cell's firing evident in the autocorrelogram. (A) has multiple small firing fields and no head-directionality. (B) has bigger and fewer firing fields and no head directionality. (C) has also big firing fields and have preferred head directionality in two directions.

4.2.2 Border cells

8 cells were categorized as border cells. All of these cells showed high firing rate field along one of the walls in the box in addition to a second firing field along the inserted wall. Of the cells categorized as border cells, there were 2 cells with some head-directionality considered to be conjunctive border x head-direction cell (Fig. 10A). 6 of the cells had no clear head-directionality (Fig.10B). Cells with firing field with some distance from wall, but still showed border vector properties, were recorded (Fig. 10C).

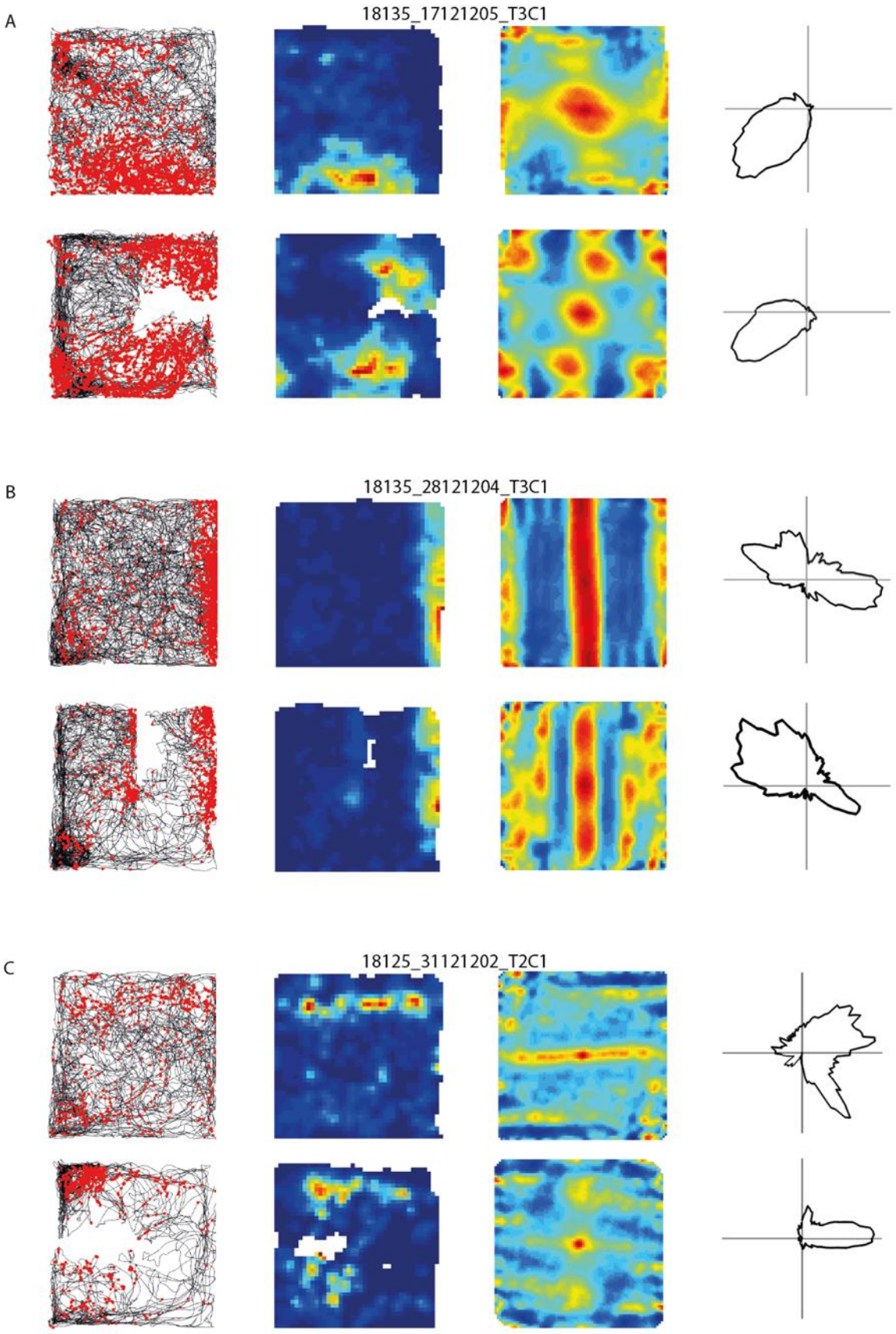
A
18135_17121205_T3C1
B
18135_28121204_T3C1
C
18125_31121202_T2C1

Fig. 10. Examples of border cells recorded in the MEC of rats running in a square enclosure. (A) From left to right: the rats running trajectory (black line) with spike locations (red dots); a color-coded rate map showing the same cell's firing distribution where the color is scaled from blue (silent) to red (peak rate); a autocorrelogram extracted from the firing rate map with color coded correlation values (blue: low correlation, red: high correlation); a polar map showing firing rate as a function of the rat's head direction with peak rate indicated. The figure arrangement in (A) is the same for (B) and (C). The upper four images is showing the result from a normal running session, while the lower four images is showing the results from a wall session, where an extra wall was inserted in the square enclosure parallel to the wall, which the cell shows high firing rate along. Please note border associated firing evident in the firing rate map for all cells: (A), (B) and (C). Also note that in the wall session images a new firing field appears along the inserted wall. (A) has a firing field close to the wall and clear head directionality. (B) has a firing field close to the wall and no clear head directionality. (C) has a firing field a bit further from the wall and some head-directionality.

4.2.3. Head-direction cells

51 cells were categorized as head-direction cells. All of these cells showed a clear preferred direction in the polar map. Of the cells recorded there were cells sharply tuned to one specific direction (Fig. 11A) and cells with wider tuning (Fig. 11B). In addition there were cells with two preferred directions (Fig. 11C).

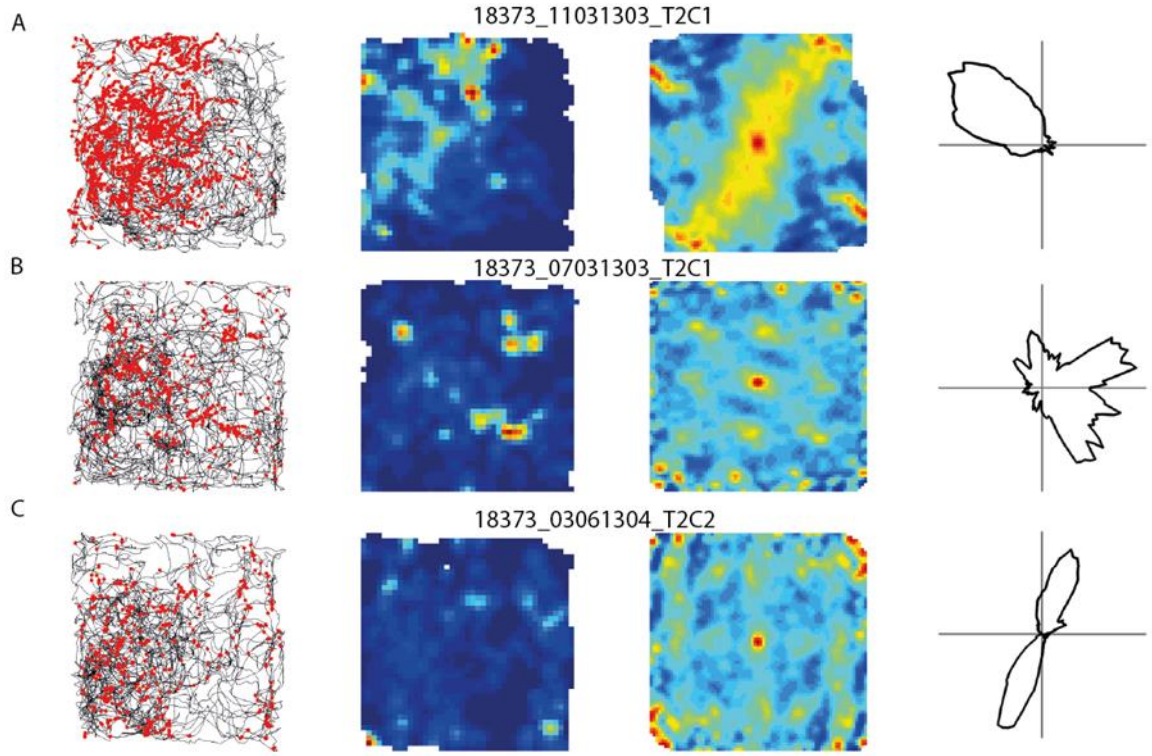

Fig. 11. Examples of head direction cells recorded in the MEC of rats running in a square enclosure. (A) From left to right: the rats running trajectory (black line) with spike locations (red dots); a color-coded rate map showing the same cell's firing distribution where the color is scaled from blue (silent) to red (peak rate); a autocorrelogram extracted from the firing rate map with color coded correlation values (blue low correlation, red high correlation); a polar map showing firing rate as a function of the rat's head direction with peak rate

indicated. The figure arrangement in (A) is the same for (B) and(C). Please note the directional modulation of cell‘s firing seen in the polar map in all (A), (B) and (C).

4.2.4 Interneurons

33 cells were categorized as head-direction cells. None of these cells showed any clear spatial or directional modulation (Fig. 12A), high firing rate and narrow waveform generated by the cell’s action potentials (Fig. 12B).

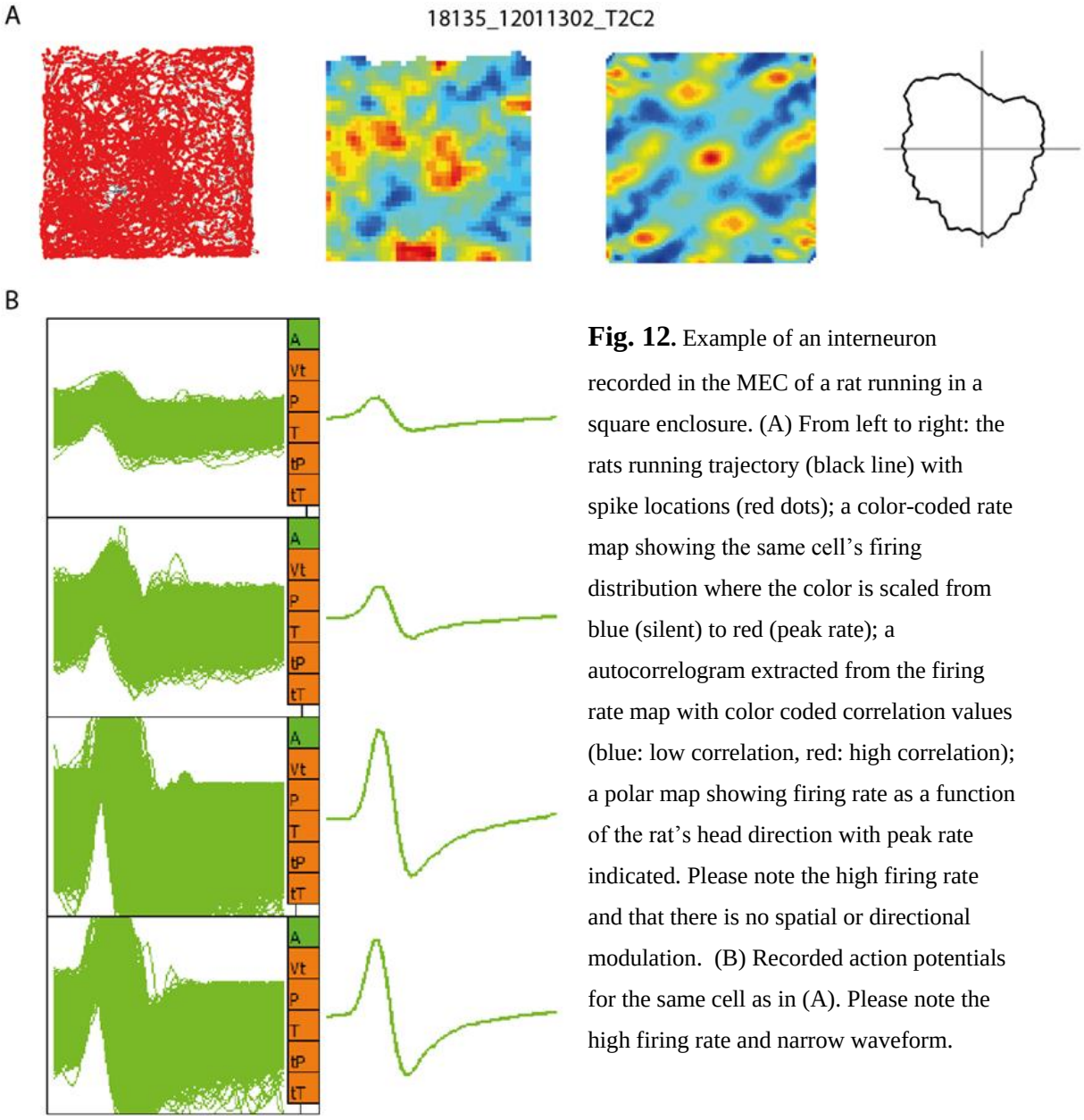

Fig. 12. Example of an interneuron recorded in the MEC of a rat running in a square enclosure. (A) From left to right: the rats running trajectory (black line) with spike locations (red dots); a color-coded rate map showing the same cell’s firing distribution where the color is scaled from blue (silent) to red (peak rate); a autocorrelogram extracted from the firing rate map with color coded correlation values (blue: low correlation, red: high correlation); a polar map showing firing rate as a function of the rat’s head direction with peak rate indicated. Please note the high firing rate and that there is no spatial or directional modulation. (B) Recorded action potentials for the same cell as in (A). Please note the high firing rate and narrow waveform.

4.3 Retrograde transduction of entorhino-entorhinal projection neurons

A retrograde gene delivering approach was applied to target projecting neurons. When a brain area injected with a virus carrying an immunohistochemical tag, the transduced neurons can later be identified both in the injection area, and by retrograde transduction in the areas that have neuron projection to the injection site. AVV viral vectors were used as the gene delivering strategy. AVV2 serotype, pseudotyped with AVV1 caspid proteins (AAV2/1), was chosen for our research. rAAV2/1 packed with pAAV-ChR2-FLAG plasmid; the ChaR2 was used for optogenetic control and FLAG is a non-florescent tag. During immunohistochemical staining, FLAG tag is bound by primary antibody which in turn is bound by a second antibody conjugated with Cy3 fluorescent dye and is used for identifying transduced neurons. A CaMKIIα promoter drove the ChR2-FLAG transcription and the construct also contain potassium channel Kir2.1 derived from 20 amino acid trafficking signal DYKDHDGDYKDHDIDYKDDDDK and ER export motif FCYNENEV (86), to improve plasma membrane localization. WPRE and BHG polyadenylation signal was included in the vector to enhance transgene transcription end expression.

rAAV2/1-ChR2-FLAG was injected into the rat's left entorhinal cortex during stereotactic surgery. After the experimental recordings were done, the rat was perfused and the brain extracted. The brain was cut into sagittal sections and immunostaining was executed to see the levels of transgene expression. Immunoflorescent images revealed ChR2-FLAG expression around the injection site in the left entorhinal cortex, and in the superficial layers of right MEC (Fig. 13). These results indicate that the that the virus was retrogradely transduced from left MEC to right MEC, as the expression is only detectable in the superficial layers of the right MEC and not anywhere else, eliminating possible passive diffusion of viral injection.

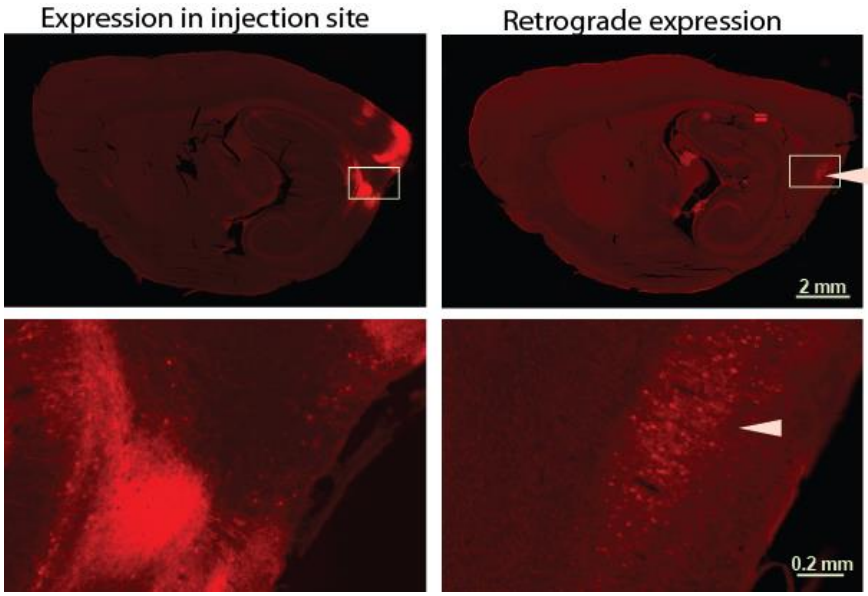

Fig. 13. ChR2-FLAG expression in MEC. Immoflourescent images of sagital brain section showing ChR2-FLAG expression in the brain. Bright red fluorescence (emission maximum at 570 nm), showing the areas which express ChR2-FLAG. The sections have been stained with immunohistochemical staining where a FLAG tag is bound by primary FLAG antibody, and then bound by a secondary antibody conjugated with Cy3 fluorescent dye. Both of the section is from the same rat: 18135. Left images are sections of the left hemisphere. Showing ChR2-FLAG expression where the virus was injected. The upper image shows the complete section. The white rectangle the upper image shows framed area in the lower image magnified. Right images are sections of the right hemisphere. Showing the ChR2-FLAG expression retrogradely transported from the injection site in the left hemisphere. The white arrow show where the recording tetrode was at its deepest position. Scale is indicated in the bottom of images where the white lines represent 2 mm and 0.2 mm.

4.4 Photoexcitation of entorhino-entorhinal projecting cells

4.4. 1. Identification of light-responsive MEC neurons

Cells with direct contralateral entorhinal projection were identified by an optogenetic approach. As mentioned, the right MEC cells were tagged by rAAV2/1-ChR2-FLAG, injected in the left MEC. The viral payload was successfully retrogradely transported to the superficial layers of MEC (Fig. 13), which leads to an expected introduction of optogenetic control over Chr2-expressing cells. The same cells recorded while the rat ran in the box (this to enable functional cell type identification as mentioned previously), was recorded in a laser stimulation session in an attempt of ChR2-activation where blue light (473nm) illuminated the cell. If the cell responded to the light (minimal firing latency after laser flash), it could be considered to have direct contralateral projection or excitatory synaptic connections to a ChR2-expressing cell, leading to indirect activation.

In the stereotactic surgery procedure, an optrode, an assembly composed of an optical fiber and four tetrodes, was implanted in the entorhinal cortex, for two of the rats only in the right MEC and four rats, both in left and right MEC. The optical fiber was 500 μm above of the tetrode tip which enabled in vivo cell activity recording and light delivery simultaneously. After running session, a laser stimulation session followed. The session took place while the rat was placed in a towel covered flower pot. Optical fibers were connected to the rats head stage for light delivery. The following recording session lasted for 2 minutes while the laser delivered 473 nm light pulses of 3.5 ms at 1Hz frequency with a power of ~25 mW (measured from the tip of the fiber). The cells recorded in the running session and laser stimulation session were considered to be the same if the isolated cluster in the scatterplot was in approximately the same position and the spike waveform shape appeared similar (Fig 14).

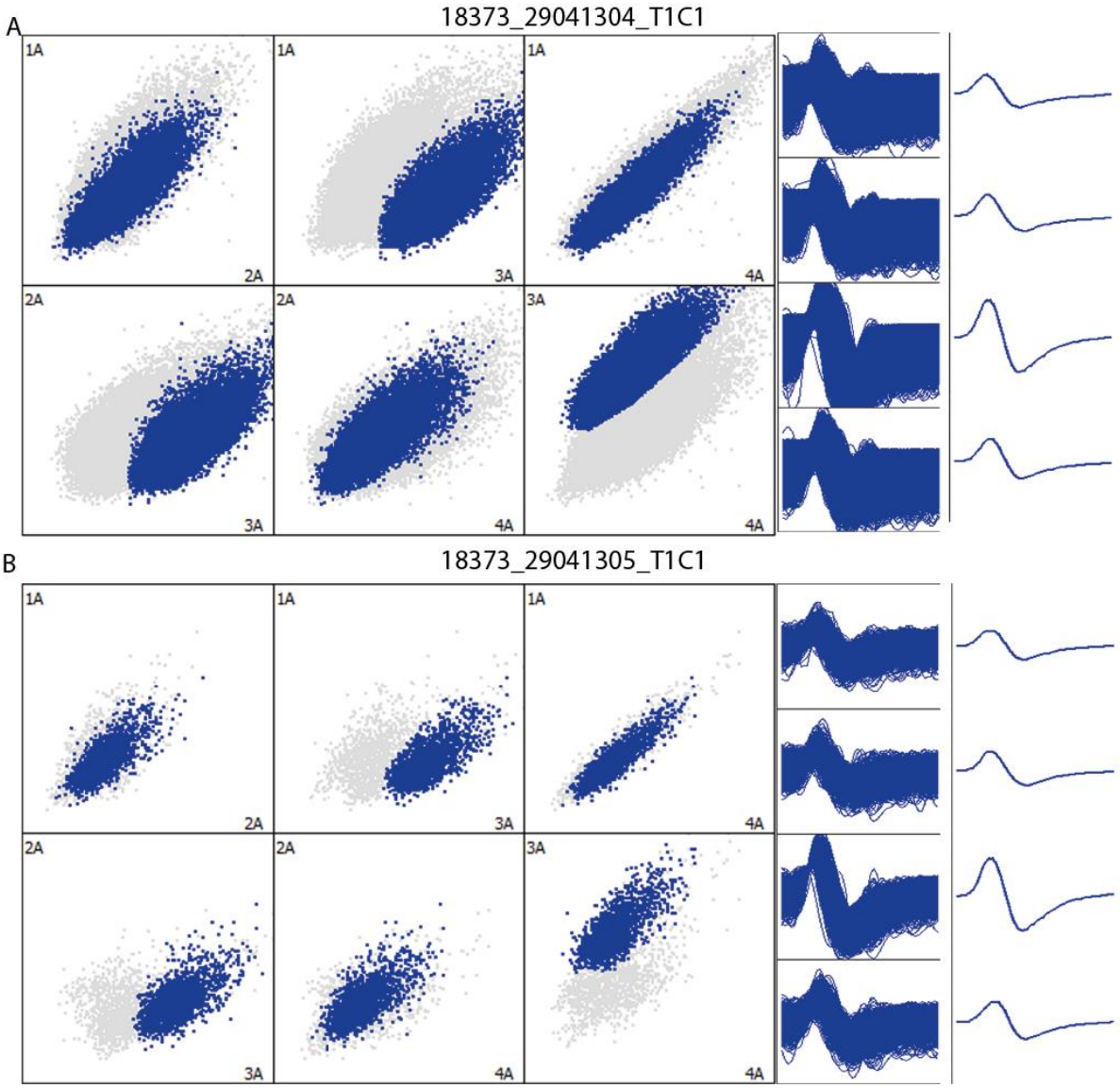

Fig. 14. The clusters and waveforms of a single recorded neuron before and during laser session. (A) Left: Electrode-pair scatterplots of neuron, before laser stimulation session. Right: Recorded action potentials from the same cell as in left. The image arrangement is the same for (B). The recording lasted for 15 min while the rat was running in the square enclosure. (B) Recorded cell during laser stimulation session. The session lasted 2 min with the rat being in the large flower pot. Please not that the clusters location looks as if it is in the same position in (A) and (B) and the waveforms look approximately the same for (A) and (B), therefore the cell recorded is considered to be the same in (A) and (B).

Spike raster and spike histograms were generated and used to determine if the neurons were light-responsive. Spike raster is showing the distribution of spikes (action potential) before and after laser stimulation. The x-axsis shows the time from the light onset (given at point 0) and the y-axsis show the number of trial, where each row represents 1 s stimulation period. A 2 min stimulation session of 1Hz stimulation will give 120 trials. If spikes are generated directly by the light activation, they will likely have the same firing latency for every laser flash. In the spike raster this will generate a vertical line of dots (each dot representing a spike) after point 0. Spike histogram showing the number of spikes plotted in accordance to their firing latency. The x-axis shows the time from light onset and ranges from – 50 to 100 milliseconds. The y-axis shows the number of spikes. If spikes are generated by the light activation, the columns in the histogram would be tallest right after point 0. Only the cells with a clear dotted line in the spike raster and clear peaks in the histogram were considered to be light-activated cells (Figs. 15-19).

32 cells were listed as responsive. Combined with an evaluation of data from the running session, identification of the functional cell type of the responsive cells was done (see paragraph: 4.2 Determining the functional identity of MEC neurons). 1 grid cell, 2 border cells, 4 head-direction cells, 7 non-spatial cells and 18 interneurons were counted as light responsive cells (Figs. 15-19).

These results suggest that combined optogenetic-electrophysiological approach can be used for determining functional identity of entorhino-entorhinal projecting MEC cell, though they do not eliminate the possibility that the light responsiveness are due to indirect stimulation of MEC neurons. Light responsiveness could arise from stimulation of ChR2 expressing MEC neurons with excitatory synapse with the cell recorded. To differentiate between direct and indirect light activated cells, the length of response latency was evaluated. The cells directly light activated should possess minimal response latencies compared to indirectly activation.

Neurons with ChR2 expression in plasma membrane will show a fast response to the laser flash, by activating ChR2 channels, whereas the synaptic activation due to light response of neighboring neurons, would take additional time.

Light responsive cells with firing latencies ~10 ms were considered to be directly activated cells. Cells with longer latencies were considered to be indirectly activated cells. These criteria for determining whether a cell is directly activated or indirectly activated, has been used in a recently published paper (42) where the same optogenetic-electrophysiological technique was used.

4.4.2 Light activated grid cell

1 light activated cell was categorized as grid cell. It had a clear grid pattern and the spike raster and spike histogram show a clear peak after point 0 (representing time of laser flash). The peaks in the two plots show longer response latency, indicating indirect activation (Fig. 15).

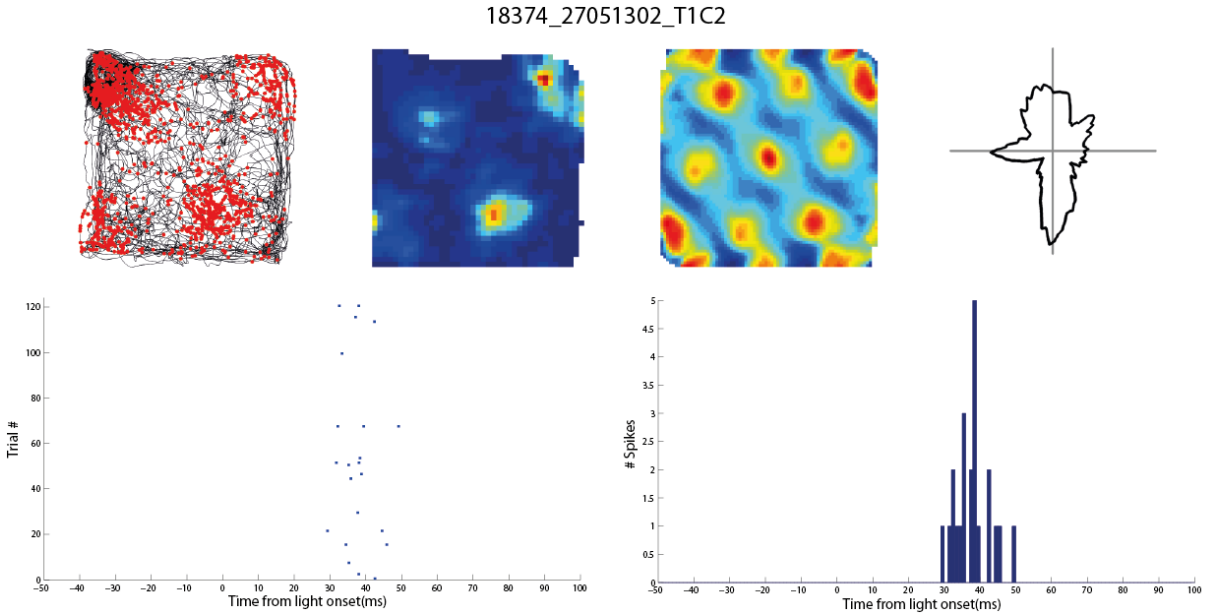

Fig. 15. Firing pattern of a light responsive grid cell recorded in MEC. The upper four images from left to right: the rats running trajectory (black line) with spike locations (red dots); a color-coded rate map showing the same cell's firing distribution where the color is scaled from blue (silent) to red (peak rate); an autocorrelogram extracted from the firing rate map with color coded correlation values (blue: low correlation, red: high correlation); a polar map showing firing rate as a function of the rat's head direction with peak rate indicated. The lower left image: spike raster showing spike distribution before and after laser stimulation (given at point 0 in the x-axis). The blue dots represent a recorded action potential from the cluster chosen. The x-axis shows the time from light onset from -50 to 100 milliseconds. The y-axis shows the trial number when the action potential

was recorded (ranging from 0 to 120 where each row represent 1 s stimulation period. 2 min stimulation session of 1Hz stimulation will give 120 trials). The lower right image: spike histogram where the number of spikes is plotted in accordance to their firing latency around the moment of stimulation (given at point 0 in the x-axis). The x-axis shows the time from light onset and ranges from – 50 to 100 milliseconds. The y-axis shows the number of spikes.

4.4.3 Light activated border cells

2 light activated cells were categorized as border cells. They had clear firing fields along the box wall (Fig. 16A) and the spike raster and spike histogram show clear peaks after point 0 (representing time of laser flash). The peaks in the two plots show a short latency of ~10 ms, indicating direct activation (Fig. 16).

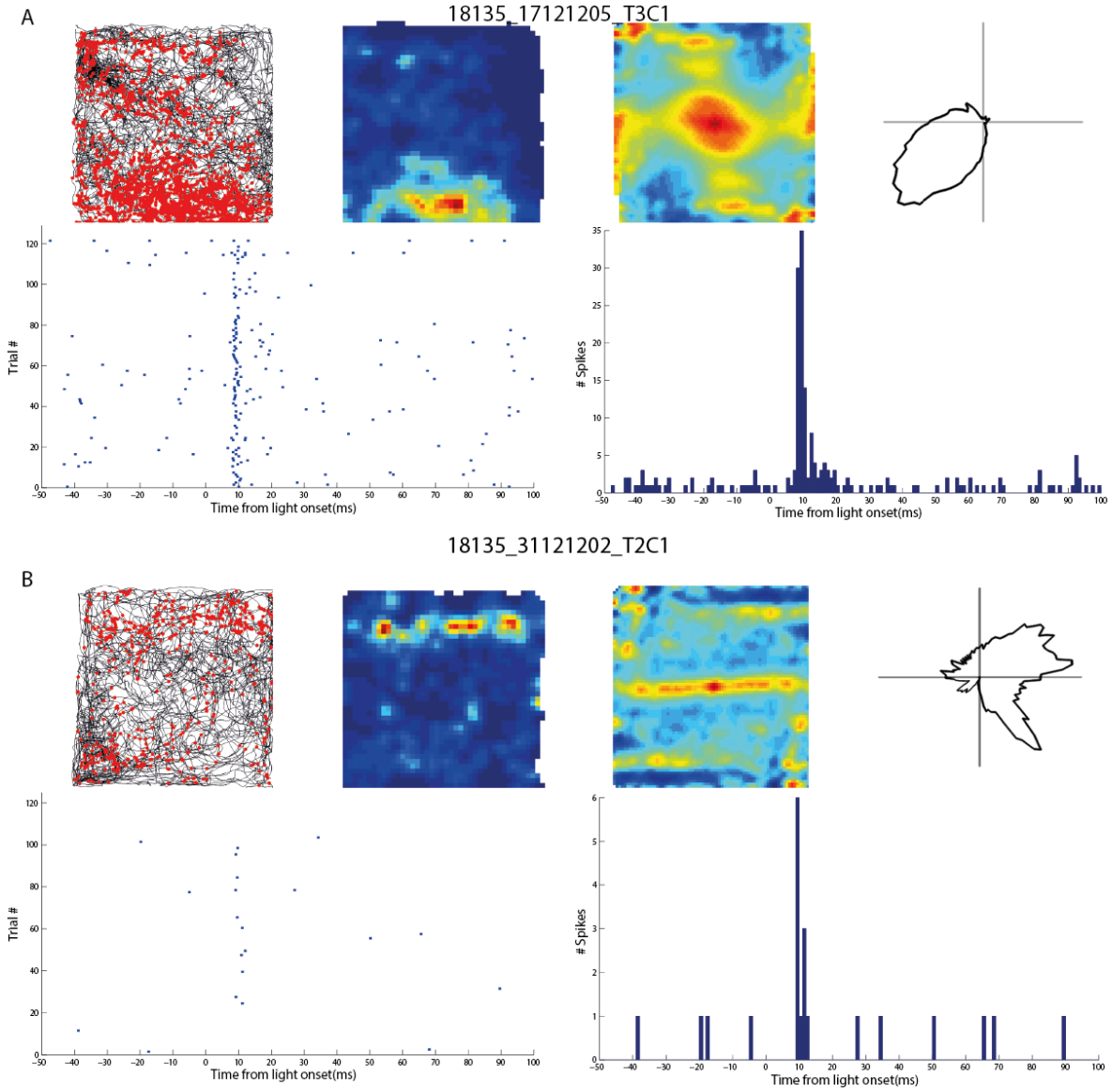

Fig. 16. Firing pattern of two laser-responsive border cells recorded in MEC. (A): The upper four images from left to right: the rats running trajectory (black line) with spike locations (red dots); a color-coded rate map showing the same cell's firing distribution where the color is scaled from blue (silent) to red (peak rate); an

autocorrelogram extracted from the firing rate map with color coded correlation values (blue: low correlation, red: high correlation); a polar map showing firing rate as a function of the rat's head direction with peak rate indicated. The lower left image: spike raster showing spike distribution before and after laser stimulation (given at point 0 in the x-axis). The blue dots represent a recorded action potential from the cluster chosen. The x-axis shows the time from light onset from -50 to 100 milliseconds. The y-axis shows the trial number when the action potential was recorded (ranging from 0 to 120 where each row represent 1 s stimulation period. 2 min stimulation session of 1Hz stimulation will give 120 trials). The lower right image: spike histogram where the number of spikes is plotted in accordance to their firing latency around the moment of stimulation (given at point 0 in the x-axis). The x-axis shows the time from light onset and ranges from – 50 to 100 milliseconds. The y-axis shows the number of spikes. The image arrangement is the same for (B).

4.4.4 Light activated head-direction cells

4 light activated cells were categorized as head-direction cells. They had a clear directional modulation (Fig. 17A) and the spike raster and spike histogram show clear peaks after point 0 (representing time of laser flash). The peaks in the two plots show a short latency of ~10 ms, for the 3 first cells presented (from top to bottom) in Fig. 17, indicating direct activation, and a longer latency for the last cell presented, indicating indirect activation (Fig. 17).

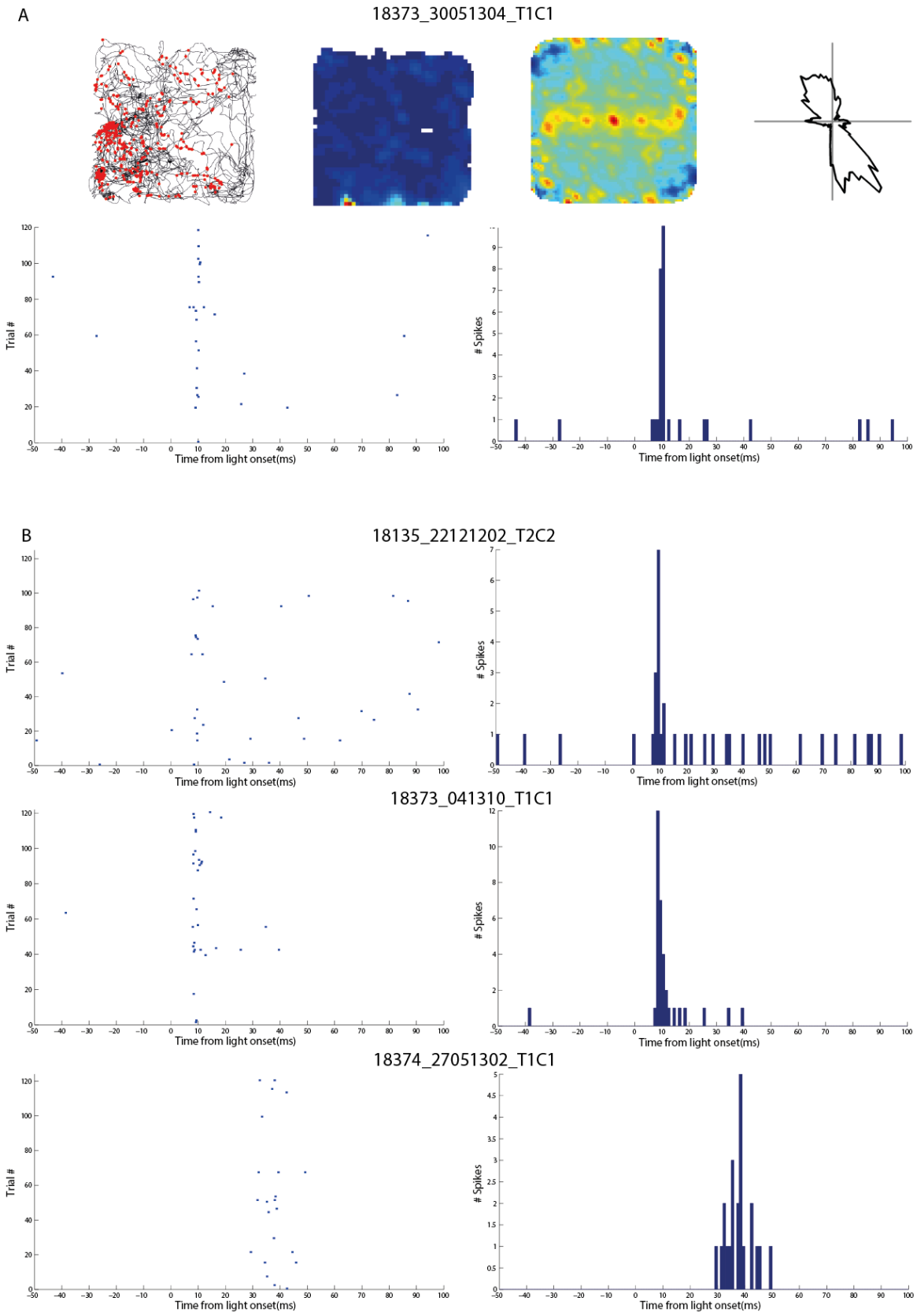
A
18373_30051304_T1C1
Trial #
Time from light onset(ms)
Spikes
Time from light onset(ms)
B
18135_22121202_T2C2
Trial #
Time from light onset(ms)
Spikes
Time from light onset(ms)
18373_041310_T1C1
Trial #
Time from light onset(ms)
Spikes
Time from light onset(ms)
18374_27051302_T1C1
Trial #
Time from light onset(ms)
Spikes
Time from light onset(ms)

Fig 17. Firing pattern of four laser-responsive head-direction cells recorded in MEC. (A) Example of laser responsive head direction cell. The upper four images from left to right: the rats running trajectory (black line) with spike locations (red dots); a color-coded rate map showing the same cell's firing distribution where the color is scaled from blue (silent) to red (peak rate); an autocorrelogram extracted from the firing rate map with color coded correlation values (blue: low correlation, red: high correlation); a polar map showing firing rate as a function of the rat's head direction with peak rate indicated. The lower left image: spike raster showing spike distribution before and after laser stimulation (given at point 0 in the x-axis). The blue dots represent a recorded action potential from the cluster chosen. The x-axis shows the time from light onset from -50 to 100 milliseconds. The y-axis shows the trial number when the action potential was recorded (ranging from 0 to 120 where each row represent 1 s stimulation period. 2 min stimulation session of 1Hz stimulation will give 120 trials). The lower right image: spike histogram where the number of spikes is plotted in accordance to their firing latency around the moment of stimulation (given at point 0 in the x-axis). The x-axis shows the time from light onset and ranges from – 50 to 100 milliseconds. The y-axis shows the number of spikes. (B) Spike raster (same as in (A) lower left) and spike histogram (same as in (A) lower right) for laser responsive head-direction cells.

4.4.5 Light activated non-spatial cells

7 light activated cells were categorized as non-spatial cells. They had no clear spatial or directional modulation and the spike raster and spike histogram show clear peaks after point 0 (representing time of laser flash) (Fig. 18A). The peaks in the two plots show a short latency of ~10 ms, for the 5 first cells presented (from top to bottom) in Fig. 18, indicating direct activation, and a longer latency for the 2 last cells presented, indicating indirect activation (Fig. 18).

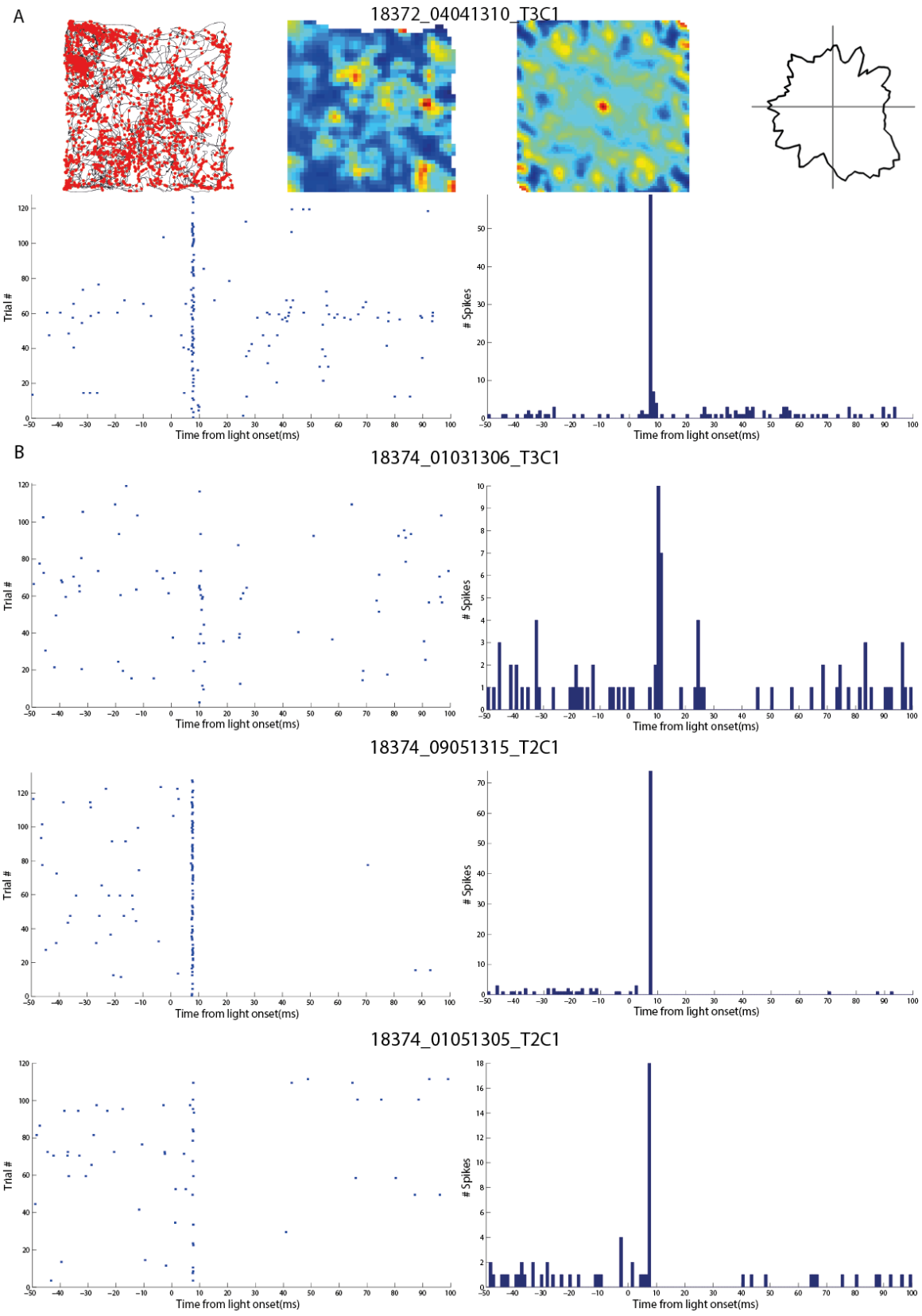
A
18372_04041310_T3C1
Trial #
Time from light onset(ms)
Spikes
Time from light onset(ms)
B
18374_01031306_T3C1
Trial #
Time from light onset(ms)
Spikes
Time from light onset(ms)
18374_09051315_T2C1
Trial #
Time from light onset(ms)
Spikes
Time from light onset(ms)
18374_01051305_T2C1
Trial #
Time from light onset(ms)
Spikes
Time from light onset(ms)

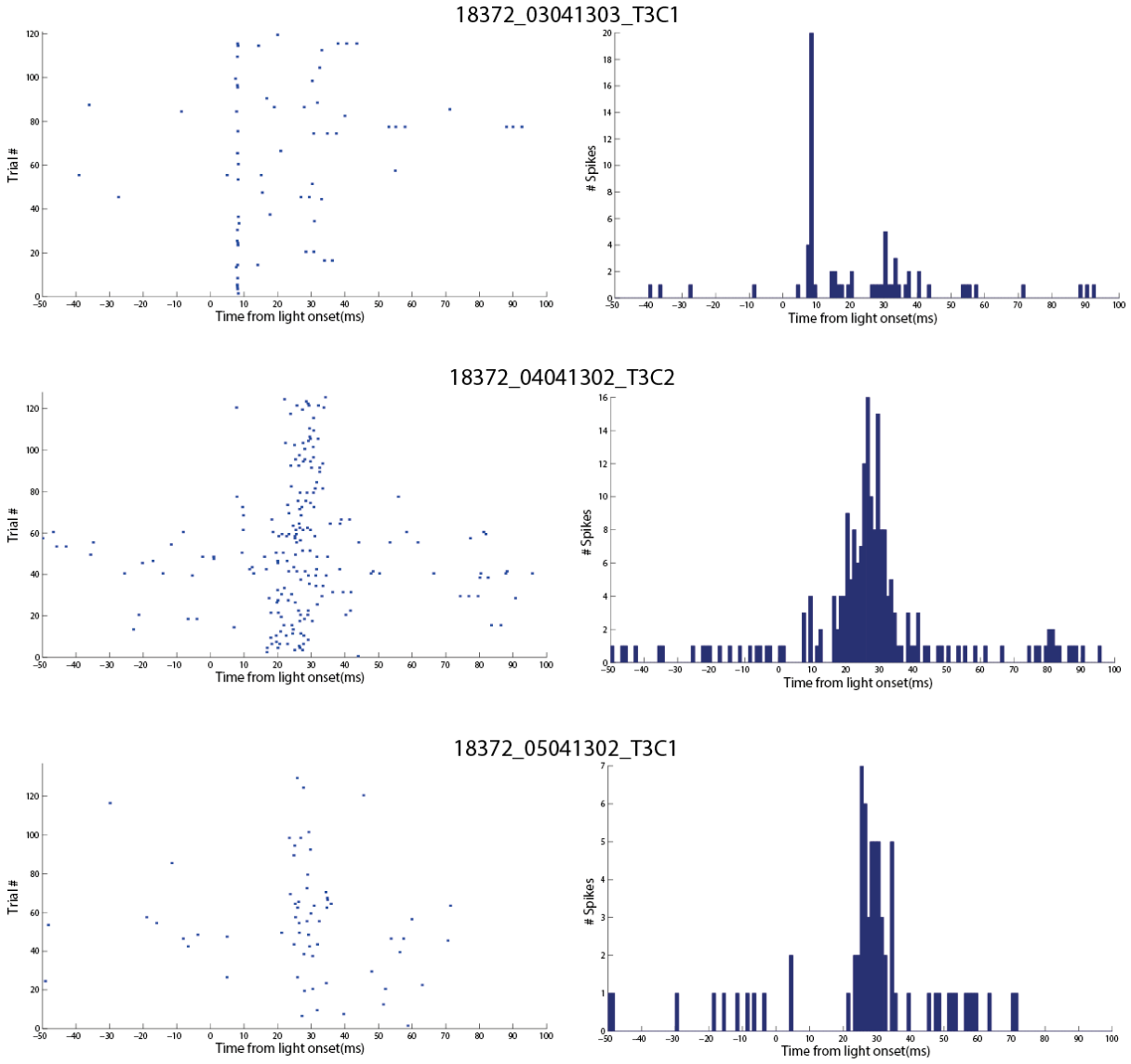

Fig. 18. Firing pattern of seven laser-responsive non-spatial cells recorded in MEC. (A): The upper four images from left to right: the rats running trajectory (black line) with spike locations (red dots); a color-coded rate map showing the same cell's firing distribution where the color is scaled from blue (silent) to red (peak rate); an autocorrelogram extracted from the firing rate map with color coded correlation values (blue: low correlation, red: high correlation); a polar map showing firing rate as a function of the rat's head direction with peak rate indicated. The lower left image: spike raster showing spike distribution before and after laser stimulation (given at point 0 in the x-axis). The blue dots represent a recorded action potential from the cluster chosen. The x-axis shows the time from light onset from -50 to 100 milliseconds. The y-axis shows the trial number when the action potential was recorded (ranging from 0 to 120 where each row represent 1 s stimulation period. 2 min stimulation session of 1Hz stimulation will give 120 trials). The lower right image: spike histogram where the number of spikes is plotted in accordance to their firing latency around the moment of stimulation (given at point 0 in the x-axis). The x-axis shows the time from light onset and ranges from – 50 to 100 milliseconds. The y-axis shows the number of spikes. (B) Spike raster (same as in (A) lower left) and spike histogram (same as in (A) lower right) for laser responsive non-spatial cells.

4.4.6 Light activated interneurons

18 light activated cells were categorized as interneurons. They had no clear spatial or directional modulation (Fig 19A) in addition to high firing rate and narrow waveform. The spike raster and spike histogram show clear peaks after point 0 (representing time of laser flash). The peaks in the two plots show a short latency of ~10 ms, for the 5 first cells presented (from top to bottom) in Fig. 19, indicating direct activation, and a longer latency for the 13 last cell presented of, indicating indirect activation.

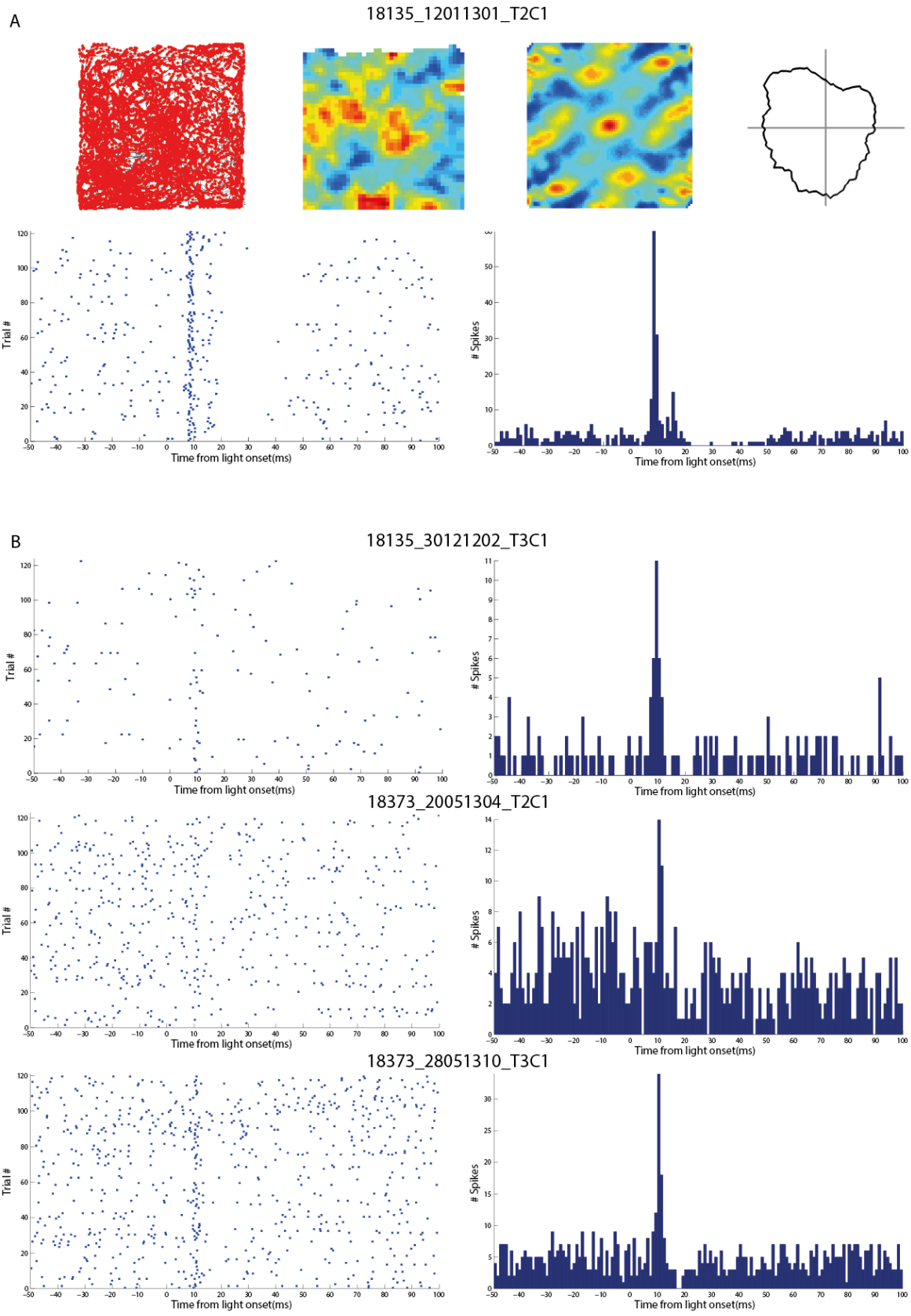
A
18135_12011301_T2C1
Trial #
Time from light onset(ms)
Spikes
Time from light onset(ms)
B
18135_30121202_T3C1
Trial #
Time from light onset(ms)
Spikes
Time from light onset(ms)
18373_20051304_T2C1
Trial #
Time from light onset(ms)
Spikes
Time from light onset(ms)
18373_28051310_T3C1
Trial #
Time from light onset(ms)
Spikes
Time from light onset(ms)

18135_30121202_T1C1

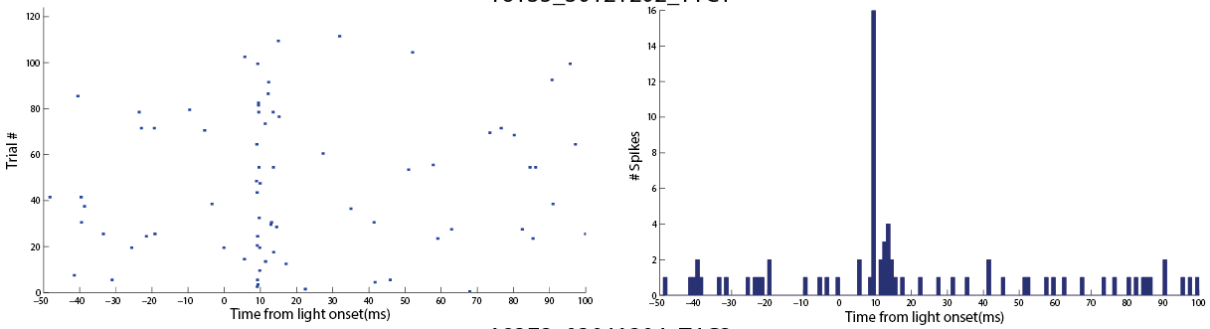

18372_03041304_T4C2

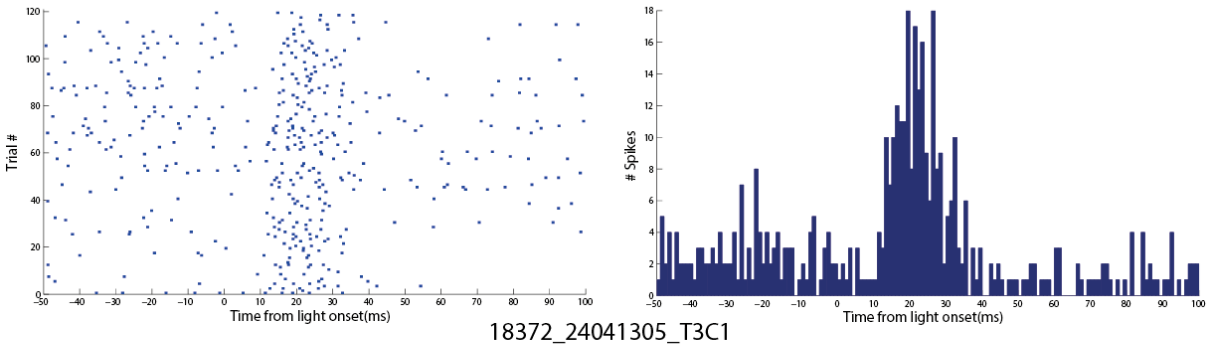

18372_24041305_T3C1

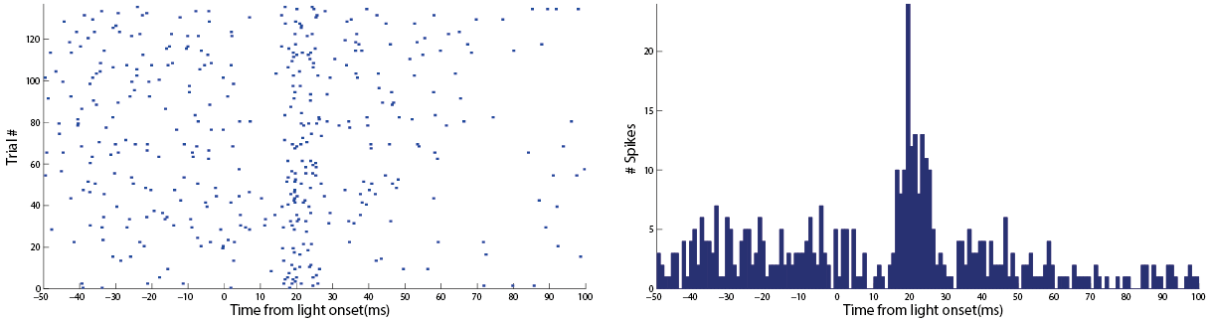

18372_02051301_T3C1

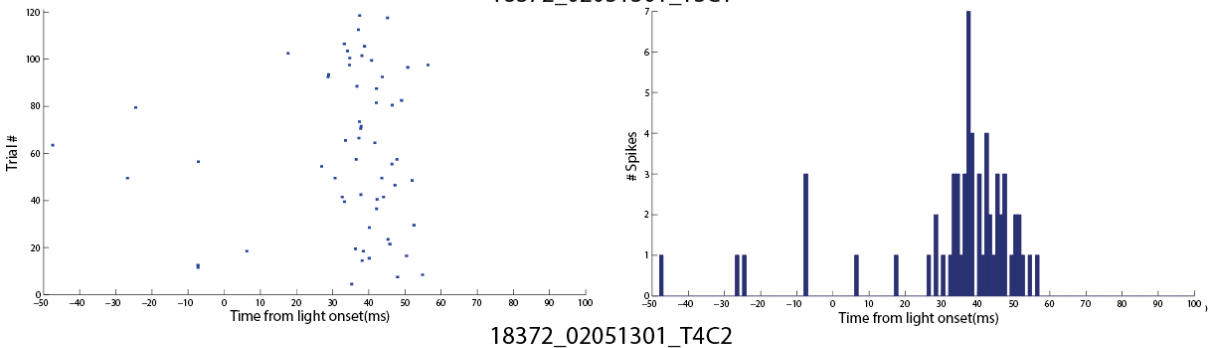

18372_02051301_T4C2

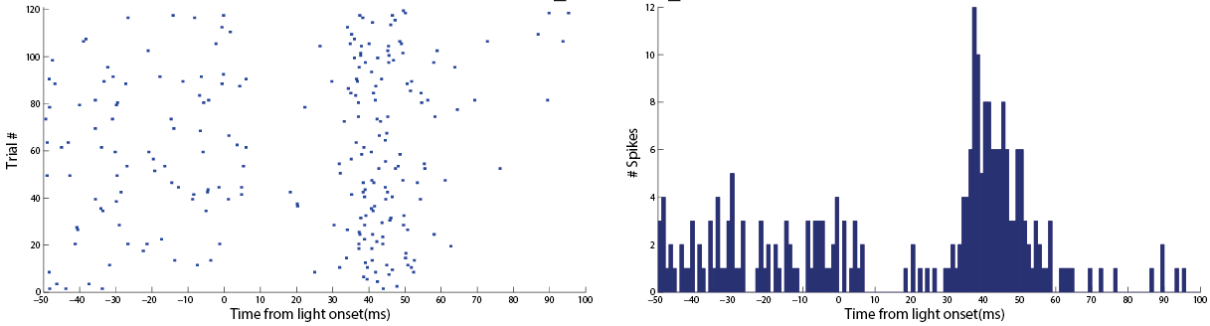

18372_06051301_T4C1

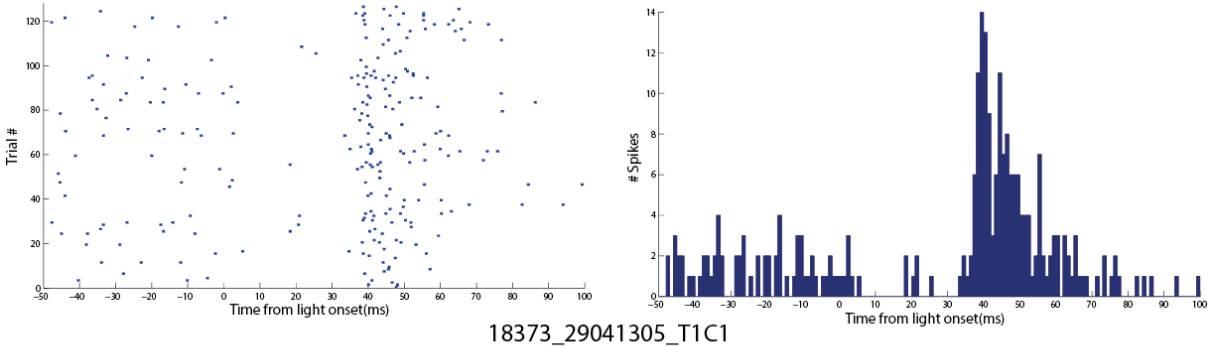

18373_29041305_T1C1

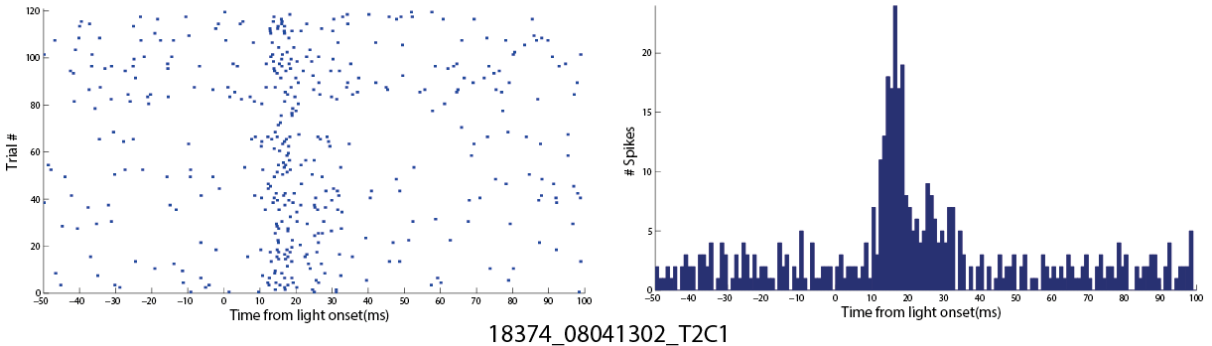

18374_08041302_T2C1

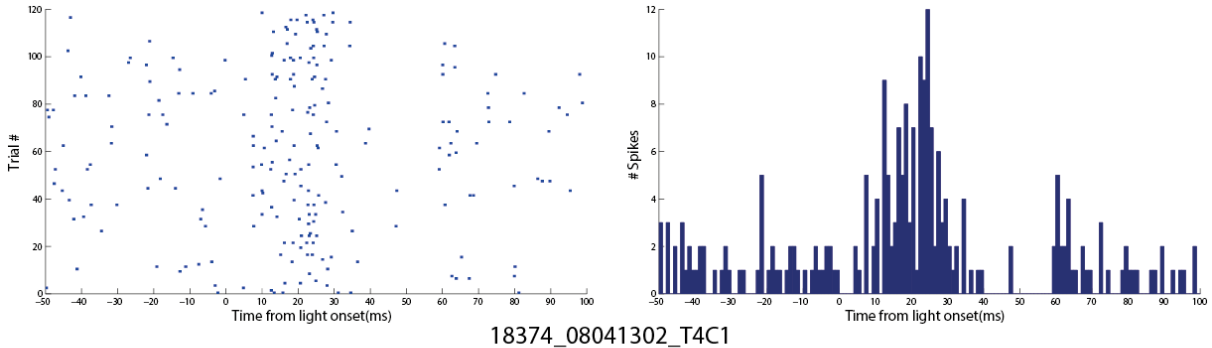

18374_08041302_T4C1

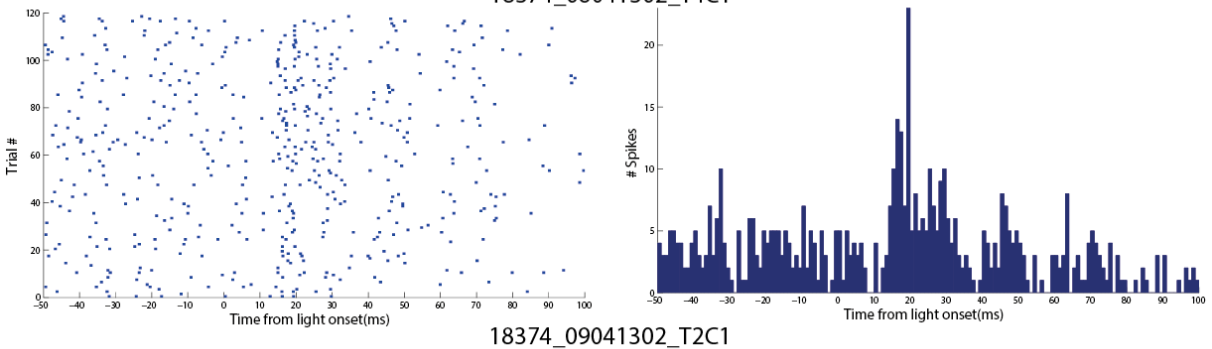

18374_09041302_T2C1

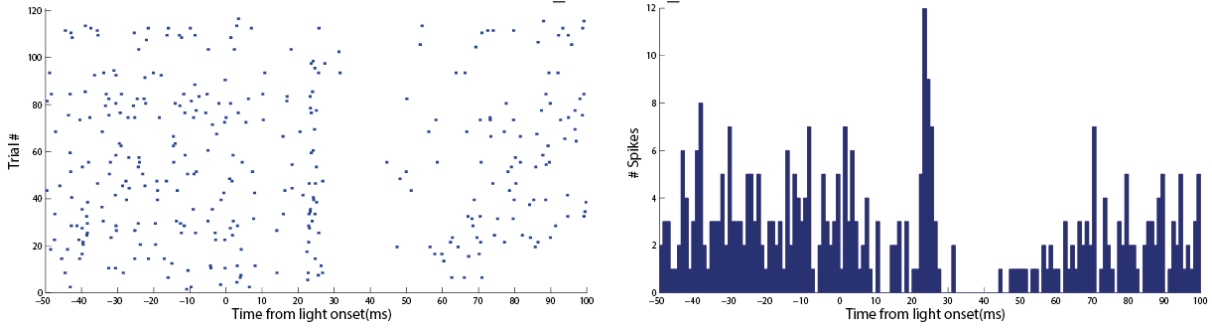

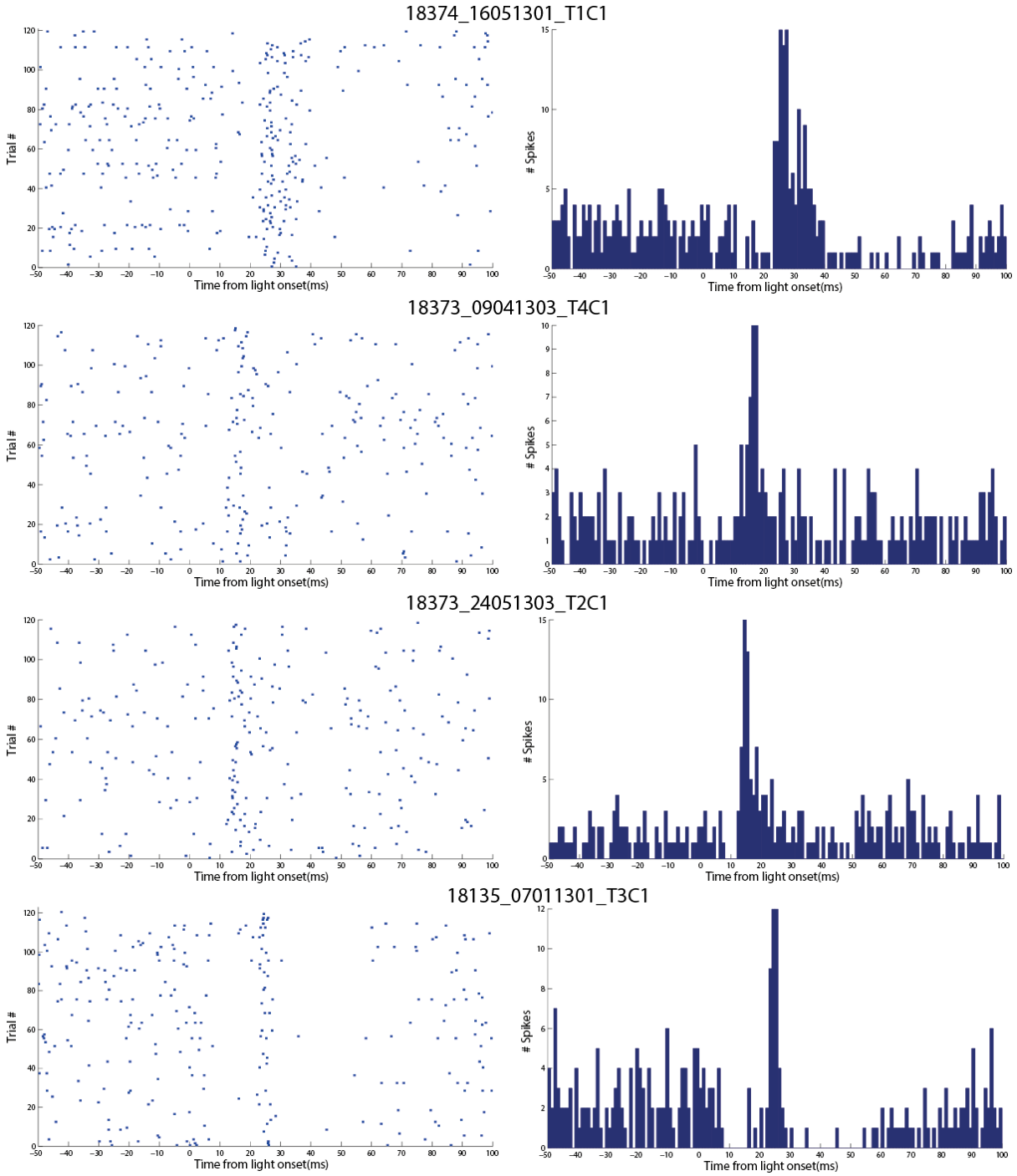

Fig. 19. Firing pattern of 18 laser-responsive interneurons cells recorded in MEC. (A) The upper four images from left to right: the rats running trajectory (black line) with spike locations (red dots); a color-coded rate map showing the same cell's firing distribution where the color is scaled from blue (silent) to red (peak rate); an autocorrelogram extracted from the firing rate map with color coded correlation values (blue: low correlation, red: high correlation); a polar map showing firing rate as a function of the rat's head direction with peak rate indicated. The lower left image: spike raster showing spike distribution before and after laser stimulation (given at point 0 in the x-axis). The blue dots represent a recorded action potential from the cluster chosen. The x-axis shows the time from light onset from -50 to 100 milliseconds. The y-axis shows the trial number when the action potential was recorded (ranging from 0 to 120 where each row represent 1 s stimulation period. 2 min

stimulation session of 1Hz stimulation will give 120 trials). The lower right image: spike histogram where the number of spikes is plotted in accordance to their firing latency around the moment of stimulation (given at point 0 in the x-axis). The x-axis shows the time from light onset and ranges from – 50 to 100 milliseconds. The y-axis shows the number of spikes. (B) Spike raster (same as in (A) lower left) and spike histogram (same as in (A) lower right) for laser responsive interneurons.

4.4.7 Latency of light activated principal cells and interneurons

The light responsive cells were grouped into putative principal cells and putative interneurons. There were in total 14 light responsive principal and 18 light responsive interneurons. The response latencies of principal cells in different sessions or animals, appear to be with minimal variation compared to response latencies of interneurons, which appear to have large variation (Fig. 20), this is in accordance to previously findings (42). It becomes clear when looking at the latency plot for principal cells (Fig. 20 left) that there are two groupings of response latencies, the largest one with short latency of about 10 ms and a smaller group with longer latency. For the interneurons (Fig. 20 right) there are only a small fraction of cells with short latency (~10ms), and the rest of the cells have longer latencies with large variations. Only the cells with latencies of ~10 ms were counted as directly light responsive cells. Cells with longer latencies were counted as indirectly activated cells. Of the cells counted as principal cells, there were 10 directly light activated cells and 4 with indirect light activation. For the cells counted as interneurons, there were 5 cells with direct light activation and 13 cells with indirect light activation. Of the principal directly light activated there were 2 border cells, 3 head-direction cells and 5 non-spatial cells.

As previously mentioned directly light activated cells suggest direct projection to the contralateral MEC. Results in this project thus indicate that border cells, head-direction cells and non-spatial cells of MEC innervate contralateral MEC by direct projections.

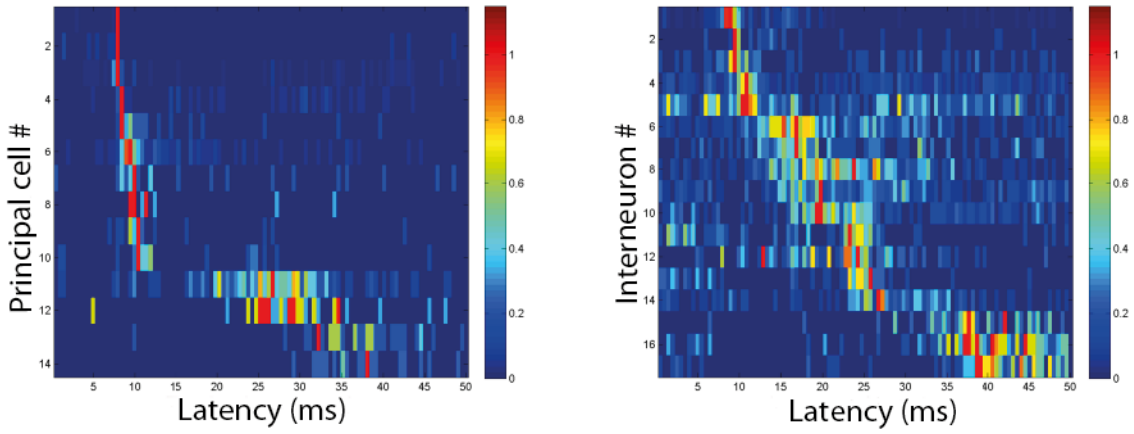

Fig. 20. Distribution of firing latencies of all light responsive principal cells and interneurons recorded in MEC. Color-coded spike rasters of MEC recorded light-responsive neurons. Spike rasters show color-coded firing rates of particular cells as a function of time after the laser stimulation. Each row in a spike raster corresponds to one cell and all the cells in one spike raster are ordered according to increasing peak response latencies; response latencies are divided into 0.5 ms time bins. Firing rates are normalized to a peak firing rate and color scale is shown on the right. Left image: Color-coded spike raster of MEC recorded light-responsive principal cells. Right image: Color-coded spike raster of MEC recorded light-responsive interneurons.

5 Discussion

5.1 Methodological considerations

In this study we chose an optogenetic combined with an electrophysiological tool to find which functional MEC neurons project to the contralateral entorhinal cortex. This approach is quite unique and can give us detailed information about neuronal connectivity. Not only will this approach enable us to target specific cells and give these cells properties so that we can control their activity by shining light on them, but we can also achieve information about their projecting pattern by using retrograde viral transduction method. We can also learn about their electrophysiological properties and determine their functional identity. Even though optogenetic-electrophysiological approach has not been used by many researchers, it has been applied with great success in a study to determine the functional MEC cell types that project to the hippocampus where the method used is exactly the same as in the project.

It would be possible to use a different methodological approach to reveal the functional cell types with entorhino-entorhinal projection; for example an electrical approach with antidromic stimulation in entorhinal cortex in one hemisphere and recording in the other. However, this method would probably not affect a large enough assembly of cells necessary to determine the functional identity of MEC cell projecting contralaterally, as only the cells with axons projecting close to the stimulation electrode would show an effect. Since all neurons of superficial layers MEC with contralateral projections were of interest in our project, an optogenetic approach was a better choice, since it probably would affect a larger population of neurons. This is evident in the immunoflourescent images showing the CHR2-FLAG transduced cells in the right hemisphere of the MEC (see Fig. 7B). A relatively large area, concentrated in the superficial layers of the MEC, showed ChR2-FLAG expression which indicate that our purpose of targeting a large number of cells in the superficial of this exact area was fulfilled.

A viral delivering tool was chosen because it leads to a fast and versatile implementation and high potency copy number linked to high gene copy number (81). An AVV vector was used because of its low toxicity, high infectivity and long-term gene expression (85), which both are properties desirable for our in vivo study. Compared to lentivirus the AVV vectors are known to have low immunogenicity which makes the transduced tissue volume lager which was a desired effect in our project. AVV is also preferred over LV in this experiment because

LV is permanently integrated into the genome of targeted cells (84) which could have lead to undesired disruption of the genes in our rats and may have interfered with the result and/or the rats' health. We chose recombinant AVV2 serotype pseudotyped with AVV1 caspid proteins, to produce AVV2/1 for our research. rAAV2/1 has shown high transduction frequencies in the CNS of the rat and has also successfully been transported retrograde in a previous study (85)

ChR2 was the opsin of chose for identifying infected neurons and it was packed along with a FLAG tag into the rAAV2/1 viral vector. Additional modifications were done (see method section) to improve transgene transcription, expression, and plasma membrane localization. After the stereotactic surgery where the virus was injected in the left MEC of 6 rats, experimental recordings followed and thereafter the rats were perfused. The brains were extracted and sliced. Some of the brain sections were Nissl stained to see the trace of the tetrodes so we could decide if the position of the recording was in the desired place (superficial layers of MEC). These sections showed that the tetrode trace were in the superficial layers of MEC, which indicated that the recorded cell activity were generated by cells in the superficial layers of MEC (see Fig. 8).

Due to limited time there was no time to do statistical analysis on the data collected. Statistical analysis applied for identification of functional cell type would increase the likelihood of correct classification of the recorded cell. Instead the cells were classified by looking at the firing distributions recorded in the running session. Whether a cell was light responsive or not was determined qualitatively. Due to time limits, statistical analysis was not performed to verify this, causing a decrease in the certainty that the cells were responsive.

5.2 All functional MEC cell types identified

In total we found about 271 cells. We classified these cells in two main categories: putative principle cells and putative interneurons. These cells were sorted by looking at the waveform, firing frequencies and firing fields. 328 cells were defined as putative principal cells and 33 as putative interneurons.

The principal cells were classified into different kinds of functional cell types based on their firing patterns. We found 72 grid cells (Fig. 11), 4 of them with head-direction modulation, known as conjunctive grid x head direction cells. We found 8 border cells (Fig. 12), two of

them were conjunctive border x head direction cells, and 51 head-direction cells (Fig. 13). A few cells had some spatial firing tendencies, but did not have the characteristic firing pattern of grid cells or border cells. These cells were classified as irregular spatial cells and we found 3 of these cells. 2 of these had only one firing field, much like the place cells of the hippocampus and have been identified in studies done by others (6, 7). In addition we found 4 cells that we counted as head direction cells, but also showed one firing field. These can be considered conjunctive head- direction x one-field cells. Also, we found cells with no spatial firing patterns, but could not be identified as interneurons as they did not have the characteristic narrow waveform or frequently firing. We categorized these cells as non-spatial cells and there were 105 of them (19A).

Previously studies have shown that interneurons have a narrower wave-form than principal cells and that their firing frequencies are higher (105). We looked also at the spatial information of all cells. Interneurons do not show any spatial information or head-direction modulation and the firing pattern is scattered evenly through the whole environment available to the rat. We found 33 cells that we categorized as interneurons based on these criteria.

The grid cells identified, had different sizes and spacing (Fig. 11). These different scaled grid cells can be regarded as cells belonging to different modules as described by recently published findings (54).

5.3 Functional cell type projecting to contralateral MEC

The findings from a recent published paper suggest that there are two different cell populations in layer II of MEC where one projects to the hippocampus and the other projects extrahippocampally (43). This led us to ask the question if the two cell populations consisted of different distributions of functional cell types. It has been shown that the population of MEC cells projecting to the hippocampus consist of all MEC functional cell types, but the major contributor is grid cells. We wanted to investigate if the distribution of functional cell types in the two subpopulations differ, and chose the contralateral MEC as termination target area based on findings suggesting strong commissural projections from MEC to MEC (13, 14). In this project the aim was to find what functional MEC cell type project to the contralateral entorhinal cortex.

In our research we found in total 32 responsive cells. 14 of them were classified as putative principal cells and 18 as putative interneurons (Fig. 20). Of the responsive putative principal cells, 1 was classified as a grid cell (see Fig. 16), 2 border cells (see Fig. 17), 4 head-direction cells (Fig.18) and 7 non-spatial cells (Fig. 19).

By looking at the spike raster and spike histogram it is evident that the different responsive cells have some variation in the response latency. 10 of the principal cells and 5 of the interneurons had short response latency of ~10 ms. These cells could be considered directly activated by the laser. 4 of the principal neurons and 13 of the interneurons had longer response latencies. Cells with long latency response are probably activated indirectly by the laser stimulation, meaning that the laser actually activates another cell with connection to the cell being recorded. The illumination of ChR2 expressing cell will lead to a depolarization of the cell which could create an action potential (spike) if this cell has an excitatory synapse with the cell recorded it would lead to a depolarization of this cell also, likely creation an action potential (spike). The response latency of the indirectly activated cells varies a lot, from about 16 ms to 40 ms, this could mean that the activation goes through more than one synapse, and that several cells could be involved, creating a polysynaptic activation. This could explain the large span between the response latency in the indirectly activated cells we found.

Of the directly laser activated cells we found 2 border cells,(Fig. 17), 3 head-direction cells (Fig. 18A-C), 5 non-spatial cells (Fig. 19A-E) and 5 interneurons all with latencies of ~10 ms (Fig. 20A-E). Directly light activated cells indicate expression of ChR2 in the cell membrane. All of these cells were recorded in the right MEC, whereas the virus containing the ChR2 was injected in the left MEC which suggests that the virus containing ChR2 has travelled through the contralateral projection retrogradely from the left MEC to the right MEC. Based on this, we can assume that all the directly laser activated cells we found do have entorhinal-entorhinal projections.

As mentioned previously, recorded cells with direct laser activation, likely to have contralateral projection, represented different functional cell type groups. We found border cells, head-direction cells, non-spatial cells and interneurons with direct laser activation, but no irregular spatial cells and no grid cells with short latency stimulation response. We did not find any responsive cells categorized as irregular spatial cells. This might be caused by a low

number of irregular cells recorded, which could lead to sampling bias. We did only collected data from 3 irregular spatial cells, which is only 1,3 % of all cells recorded.

What is more interesting is the fact that we did not find any grid cells with direct laser activation. We found only one light activated grid cell, but this with indirect activation (Fig. 16). In contrast to the low number of irregular spatial cells found, the number of grid cells was quite high. We found 72 grid cells, which is 31.5% of all cells recorded and none of them were considered to have contralateral projection. This could also be caused by limited sampling (only form 6 rats and only 270 cells). To draw the conclusions that grid cells in the superficial layers of MEC do not project to the contralateral MEC, all neurons of this particular population need to be investigated. With the research tools available today, this could be quite challenging. In spite of this, based on the number of grid cells found and the fact that we were able to find cells from other functional cell type groups with direct light activation, it could be speculated that all functional MEC cell types, projects contralaterally to the MEC, except the grid cells. This distribution of functional cell types would be in contrast to the distribution of functional cell types shown to project to the hippocampus (42). To investigate whether the sparsity of light responsive grid cells are due to limited sampling or if it indicates a different distribution of functional cell types in the cell population projecting contralaterally vs. the hippocampus, further research is needed.

6. Conclusion

This thesis sheds light on the functional cell type distribution in superficial layers of MEC projecting contralaterally to the MEC. By using a retrograde gene delivery strategy, entorhino-entorhinal projecting MEC cells were tagged. A combined optogenetic-electrophysiological approach allowed us to determine the functional identity of these cells. The results indicate the presence of at least four different functional MEC cell types with the contralateral MEC as their projection target. Border cells, head-direction cells, non-spatial cells and interneurons were all found to have this particular projection.

It has been shown that the functional cell types of superficial layers of MEC with projection to the hippocampus in a large part consist of grid cells. Although multiple grid cells were identified in our project, none of them satisfied the criteria set to be considered to have direct projection to the contralateral MEC. This is in contrast to the distribution of functional MEC cell types projecting to the hippocampus. Whether these results are caused by limited sampling, or if they suggest that the contralaterally projecting cell population and the cell population projecting to the hippocampus has distinct functional properties, remains unknown. To answer this question further research is acquired.

References

1. E. C. Tolman, Cognitive maps in rats and men. *Psychol. Rev.* **55**, 189 (1948).

2. E.C. Tolman, B.F. Ritchie, D. Kalish, Studies in spatial learning: Orientation and the short-cut *J. Exp. Psychol.* **36**, 13 (1946).

3. J. O'Keefe, J. Dostrovsky, The hippocampus as a spatial map. Preliminary evidence from unit activity in the freely-moving rat. *Brain Res.* **34**, 171 (1971).

4. V. H. Brun et al., Place cells and place recognition maintained by direct entorhinal-hippocampal circuitry. *Science* **296**, 2243 (2002).

5. E. I. Moser, M.-B Moser, A metric for space. *Hippocampus* **18**, 1142 (2008).

6. F. Sargolini et al., Conjunctive representation of position, direction, and velocity in entorhinal cortex. *Science* **312**, 758 (2006).

7. F. Savelli, D. Yoganarasimha, J. J. Knierim, Influence of boundary removal on the spatial representations of the medial entorhinal cortex. Hippocampus 18, 1270 (2008).

8. T. Hafting, M. Fyhn, S. Molden, M.-B. Moser, E. I. Moser, Microstructure of a spatial map in the entorhinal cortex. *Nature* **436**, 801 (2005).

9. M. P. Witter, D. Amaral, in *Hippocampal Formation. The Rat Nervous System.* (G. Paxinos. Amsterdam, 2004) pp. 635-704.

10. N. M. van Strien, N. L. M. Cappaert, M. P. Witter, The anatomy of memory: an interactive overview of the parahippocampal-hippocampal network. *Nat. Rev. Neurosci.* **10**, 272 (2009).

11. D.G. Amaral, P. Lavenex, in *Hippocampal Neuroanatomy. The Hippocampus Book.* (Oxford University Press. Oxford, 2004) pp. 37-131.

12. C. Köler, Intrinsic connections of the retrohippocampal region in the rat brain II. The medial entorhinal area. *J. Comp. Neurol.* **246**, 149 (1986).

13. C. Köler, Intrinsic connections of the retrohippocampal region in the rat brain III. The medial entorhinal area. *J. Comp. Neurol.* **271**, 208 (1988).

14. J. O'Keefe, L. Nadel, in *The hippocampus as a cognitive map*. (Clarendon Press, Oxford,1978).

15. D. Derdikman, E. I. Moser, A manifold of spatial maps in the brain. *Trends in Cognitive Sciences* **14**, 561 (2010).

16. R. F. Langston, et al., Development of the spatial representation system in the rat. *Science* **328**, 1576 (2010).

17. T. J. Wills, F. Cacucci, N. Burgess, J. O'Keefe, Development of the hippocampal cognitive map in preweanling rats. *Science* **328**, 1573 (2010).

18. G. J. Quirk, et al., The firing of hippocampal place cells in the dark depends on the rats recent experience. *J. Neurosci.* **10**, 2008 (1990).

19. R. U Muller, J. L Kubie, E. M. Bostock, J. S. Taube, G. J. Quirk, in *Spatial firing correlates of neurons in the hippocampal formation of freely moving rats*. (Oxford University Press, New York, 1991) pp 296–333.

20. R. Muller, J. Kubie, The effects of changes in the environment on the spatial firing of hippocampal complex-spike cells. *J. Neurosci.***7**, 1951 (1987).

21. E. Bostock , R. U. Muller, J. L. Kubie, Experience-dependent modifications of hippocampal place cell firing. *Hippocampus* **1**, 193 (1991).

22. E. J. Markus, Y. L. Qin, B. Leonard, W. E. Skaggs, B. L. McNaughton, C. A. Barnes, Interactions between location and task affect the spatial and directional firing of hippocampal neurons. *J. Neurosci.* **15**, 7079 (1995).

23. L. L. Colgin, E. I. Moser, M.-B. Moser, Understanding memory through hippocampal remapping. *Trends Neurosci.* **31**, 469 (2008).

24. D. S. Touretzky, A. D. Redish, Theory of rodent navigation based on interacting representations of space. *Hippocampus* **6**, 247 (1992).

25. M. Fyhn, S. Molden, M. P. Witter, E. I. Moser, M.-B. Moser, Spatial Representation in the Entorhinal Cortex. *Science* **305**, 1258 (2004).

26. V. H. Brun *et al.*, Impaired Spatial Representation in CA1 after Lesion of Direct Input from Entorhinal Cortex. *Neuron* **57**, 290 (2008).

27. M. C. Fuhs, D. S. Touretzky, A spin glass model of path integration in rat medial entorhinal cortex. *J. Neurosci.* **26**, 4266 (2006).

28. B. L. McNaughton, F. P. Battaglia, O. Jensen, E. I. Moser, M.-B. Moser, Path integration and the neural basis of the 'cognitive map'. *Nat. Rev. Neurosci.* **7**, 663 (2006).

29. T. Solstad, E. I. Moser, G. T. Einevoll, From grid cells to place cells: A mathematical model. *Hippocampus* **16**, 1026 (2006).

30. T. Solstad, C. N. Boccara, E. Kropff, M.-B. Moser, E. I. Moser, Representation of Geometric Borders in the Entorhinal Cortex. *Science* **322**, 1865 (2008).

31. P. A. Naber, M. Caballero-Bleda, B. Jorritsma-Byham, M. P. Witter, Parallel input to the hippocampal memory system through peri- and postrhinal cortices. *NeuroReport* **8**, 2617 (1997).

32. C. B. Canto, F. G. Wouterlood, M. P. Witter, What Does the Anatomical Organization of the Entorhinal Cortex Tell Us? *Neural Plasticity* **2008**, Article ID 381243 (2008).

33. R. Klink, A. Alonso, Morphological characteristics of layer II projecton neurons in the rat medial entorhinal cortex. *Hippocampus* **7**, 571 (1997).

34. B. Tahvildari , A. Alonso, Morphological and electrophysiological properties of lateral entorhinal cortex layers II and III principal neurons. *J. Comp. Neurol.* **491**, 123 (2005).

35. T. van Haeften, F. G. Wouterlood, B. Jorrisma-Byham, M. P. Witter, GABAergic presubicular projections to the medial entorhinal cortex of the rat. *J. Neurosci.* **17**, 862 (1997)

36. T. van Haeften, B. Jorritsma-Byham, M. P. Witter, Quantitative morphological analysis of subicular terminals in the rat entorhinal cortex. *Hippocampus* 5, 452 (1995).

37. A. Pinto, C. Fuentes, D. Paré, Feedforward inhibition regulates perirhinal transmission of neurocortical inputs to the entorhinal cortex: ultrastructural study in guinea pigs. *J. Comp. Neurol.* **495**, 722 (2006).

38. B. F. Jones, M. P. Witter, Cingulate cortex projections to the parahippocampal region and hippocampal formation in the rat. *Hippocampus* **17**, 957 (2007).

39. E. A. Tolner, F. Kloosterman, E. A. van Vliet, M. P. Witter. F H. Silva, J. A. Gorter, Presubiculum stimulation in vivo evokes distinct oscillations in superficial and deep entorhinal cortex layers in chronic epileptic rats. *J. Neurosci.* **25**, 8755 (2005).

40. B. N. Hamam, T. E. Kennedy, A. Alonso, D. G. Amaral, Morphological and electrophysiological characteristics of layer V neurons of the rat medial entorhinal cortex. *J. comp. Neurol.* **418**, 457 (2000).

41. E. I. Moser, M. –B. Moser, in *Handbook of Brain Microcircuits*, G. Shepherd, S. Grillner, Eds. (Oxford University Press, USA, 2010) pp. 175-186

42. S.–J. Zhang et al., Optogenetic dissection of entorhinal-hippocampal functional connectivity. *Science* **340**, Article ID 1232627 (2013).

43. C. Varga, S. Y. Lee, I. Soltesz, Target-selective GABAergic control of entorhinal cortex output. *Nat. Neurosci.* **13**, 822 (2010).

44. G. Adelmann, T. Deller, M. Frotscher, Organization of identified fiber tracts in the rat fimbria-fornix: an anterograde tracing and electron microscopic study. *Anat. Embryol.* **193**, 481 (1996).

45. L. M. Giocomo, M. –B. Moser, E. I. Moser, Computational models of grid cells. *Neuron* **71**, 589 (2011).

46. E. T. Rolls, S. M. Stringer, T. Elliot, Entorhinal cortex grid cells can map to hippocampal place cells by competitive learning. *Network* **17**, 447 (2006).

47. T. J McHugh, K. I. Blum, J Z Tsien, S. Tonegawa, M. A. Wilson, Impaired hippocampal representation of space in CA1-specific NMDAR1 knockout mice. *Cell* **87**, 1339 (1996).

48. S. Leutgeb, J. K. Leutgeb, A.Treves, M. –B. Moser, E. I. Moser, Distinct ensemble codes in hippocampal areas CA3 and CA1. *Science* **305**, 1295 (2004).

49. J. O'Keefe, N. Burgess, Dual phase and rate coding in hippocampal place cells: Theoretical significance and relationship to entorhinal grid cells. *Hippocampus* **15**, 853 (2005).

50. N. Burgess, C. Barry, J. O'Keefe, An oscillatory interference model of grid cell firing. *Hippocampus* **17**, 801 (2007).

51. L. M. Giocomo, E. A. Zilli, E. Fransén, M. E. Hasselmo, Temporal frequency of subthreshold oscillations scales with entorhinal grid cell field spacing. *Science* **315**, 1719 (2007).

52. X. –J. Wang, in *Encyclopedia of Neuroscience*, volume 1, 667-679. (Academic Press, Oxford, 2010) pp .667-679.

53. K. Zhang,Representation of spatial orientation by the intrinsic dynamics of the head-direction cell ensemble: a theory. *J. Neurosci.* **16**, 2112 (1996).

54. H. Stensola *et al.*, The entorhinal grid map is discretized. *Nature* **492**, 72 (2012).

55. G. Nagel *et al.*, Channelrhodopsin-1: a light-gated proton channel in green algae. *Science* **296**, 2395 (2002).

56. G. Nagel *et al.*, Channelrhodopsin-2, a directly light-gated cation-selective membrane channel. *Proc. Natl. Acad. Sci*. **100**, 13940 (2003).

57. E. S. Boyden, F. Zhang, E. Bamberg, G. Nagel, K. Deisseroth, Millisecond-timescale, genetically targeted optical control of neural activity. *Nat. Neurosci.* **8**, 1263 (2005).

58. K. Deisseroth, G. Feng , A. K. Majewska, G. Miesenbock, A. Ting, M. J. Schnitzer, Next-generation optical technologies for illuminating genetically targeted brain circuits. *J. Neurosci.* **26**, 10380 (2006).

59. M. Rein, J. Deussing, The optogenetic (r)evolution. *Mol. Genets. Genomics* **287**, 95 (2012).

60. F. H. Crick, Thinking about the brain. *Sci. Am.* **241**, 219 (1979).

61. D. Oesterhelt, W. Stoeckenius, Rhodopsin-like protein from the purple membrane of Halobacterium halobium. *Nat. New Biol.* **233**: 149 (1971).

62. R. L. Fork, Laser stimulation of nerve cells in Aplysia. *Science* **171**, 907 (1971).

63. A. Grinvald , A. Fine A, I. C. Farber, R. Hildesheim . Fluorescence monitoring of electrical responses from small neurons and their processes. *Biophys. J.* **42**, 195 (1983).

64. D. Shmucker, A. L Su, A. Beermann, H Jäkle, D. G. Jay, Chromophore-assisted laser inactivation of patched protein switches cell fate in the larval visual system of Drosophila. *Proc. Natl. Acad. Sci.* 91, 2664 (1994).

65. A. Matsuno-Yagi, Y. Mukohata, Two possible roles of bacteriorhodopsin; a comparative study of strains of Halobacterium halobium differing in pigmentation. *Biochem. Biophys. Res. Commun.* **78**, 237 (1977).

66. Y. Mei, F. Zhang, Molecular Tools and Approaches for Optogenetics. *Biol. Psychiatry* **71**, 1033 (2012).

67. J. L. Spudich, C.-S. Yang, K.-H. Jung, E. N. Spudich, Retinylidene proteins: structures and functions from archaea to humans. *Annu. Rev. Cell Biol.* **16**, 365 (2000).

68. J. L. Spudich, The multitalented microbial sensory rhodopsins. *Trends Microbiol.* **14**, 480 (2006).

69. U. Haupts, J. Tittor, E. Bamberg, D. Oesterhelt, General concept for ion translocation by halobacterial retinal proteins: The isomerization/switch/transfer (IST) model. *Biochemistry* **36**, 2 (1997).

70. E. S. Boyden, F. Zhang, E. Bamberg, G. Nagel, K. Deisseroth, Millisecond-timescale, genetically targeted optical control of neural activity. *Nat Neurosci* **8**, 1263 (2005).

71. F. Zhang, L. P. Wang, E. S. Boyden, K. Deisseroth, Channelrhodopsin-2 and optical control of excitable cells. *Nat. Methods* **3**, 785 (2006).

72. F. Zhang, A. M. Aravanis, A. Adamantidis, L. de Lecea, K. Deisseroth, Circuit-breakers: optical technologies for probing neural signals and systems. *Nat. Rev. Neurosci.* **8**, 577 (2007).

73. T. Ishizuka, M. Kakuda, R. Araki, H. Yawo, Kinetic evaluation of photosensitivity in genetically engineered neurons expressing green algae light-gated channels. *Neurosci. Res.* **54**, 85 (2006).

74. T. P. Sakmar, Structure of rhodopsin and the superfamily of sevenhelical receptors: the same and not the same. *Curr. Opin. Cell Biol.* **14**, 189 (2002).

75. Y. Shichida, T. Yamashita, Diversity of visual pigments from the viewpoint of G protein activation—comparison with other G protein-coupled receptors. *Photochem. Photobiol. Sci.* **2**, 1237 (2003).

76. J. Y. Lin, M. Z. Lin, P. Steinbach, R. Y. Tsien, Characterization of engineered channelrhodopsin variants with improved properties and kinetics. *Biophys. J.* **96**, 1803 (2009).

77. S. P. Tsunoda, P. Hegemann, Glu 87 of channelrhodopsin-1 causes pH-dependent color tuning and fast photocurrent inactivation. *Photochem. Photobiol.* **85**, 564 (2009).

78. J. P. Britt, R. A. McDevitt, A Bonci, Use of channelrhodopsin for activation of CNS neurons. *Curr. Protoc. Neurosc* . Ch. 2:Unit2.16 (2012)
.

79. M. Favero, Synaptic cooperativity regulates persistent network activity in neocortex. *J. Neurosci.* **33**, 3151 (2013).

80. E. Krook-Magnuson, C. Armastrong, C Oijala, I. Soltez, On-demand optogenetic control of spontaneous seizures in temporal lobe epilepsy. *Nat. Commun.* **4**, 1376 (2013).

81. O. Yizhar *et al.*, Neocortical excitation/inhibition balance in information processing and social dysfunction. *Nature* **477**, 171 (2011).

82. T Dittgen et al., Lentivirus-based genetic manipulations of cortical neurons and their optical and electrophysiological monitoring in vivo. *Proc. Natl. Acad. Sci.* 28, 101 (2004).

83. P. E. Monahan, R. J. Samulski, Adeno-associated virus vectors for gene therapy: more pros than cons? *Mol. Med. Today* **6**, 433 (2000).

84. F. Zhang, et al., Optogenetic interrogation of neural circuits: technology for probing mammalian brain structures. *Nat. Protoc.* **5**,439 (2010).

85. C. Burger *et al.*, Recombinant AAV Viral Vectors Pseudotyped with Viral Capsids from Serotypes 1, 2, and 5 Display Differential Efficiency and Cell Tropism after Delivery to Different Regions of the Central Nervous System. *Mol. Ther.* **10**, 302 (2004).

86. V. Gradinaru *et al.*, Molecular and Cellular Approaches for Diversifying and Extending Optogenetics. *Cell* **141**, 154 (2010).

87. V. Gradinaru, et al., Targeting and readout strategies for fast optical neural control in vitro and in vivo. *J. Neurosci.* **27**,14231 (2007).

88. V. Gradinaru, M. Mogri, K. R. Thompson, J. M. Henderson, K. Deisseroth, Optical deconstruction of parkinsonian neural circuitry. *Science* **324**, 354 (2009).

89. I. R. Wickersham, et al., Monosynaptic restriction of transsynaptic tracing from single, genetically targeted neurons. *Neuron* **53**, 639 (2007).

90. U. Maskos, K. Kissa, C. St Cloment, P. Brûlet, Retrograde transsynaptic transfer of green fluorescent protein allows the genetic mapping of neuronal circuits in transgenic mice. *Proc Natl. Acad. Sci.* **99**, 10120 (2002).

91. M. Sugita, Y. Shiba, Genetic tracing shows segregation of taste neuronal circuitries for bitter and sweet. *Science* **309**, 781 (2005).

92. E. M. Callaway, Transneuronal circuit tracing with neurotropic viruses. Neurons with vesicular stomatitis virus vectors. *Proc. Natl. Acad. Sci.* **108**, 15414 (2008).

93. K. T. Beier, et al., Anterograde or retrograde transsynaptic labeling of CNS neurons with vesicular stomatitis virus vectors. *Proc. Natl. Acad. Sci.* **108**, 15414 (2011).

94. B. R. Arenkiel, et al., In vivo light-induced activation of neural circuitry in transgenic mice expressing channelrhodopsin-2. *Neuron* **54**, 205 (2010).

95. S. Zhao, et al., Celltype-specific channelrhodopsin-2 transgenic mice for optogenetic dissection of neural circuitry function. *Nat. Methods* **8**, 745 (2011).

96. L. Petreanu, D. Huber, A. Sobczyk, K. Svoboda, Channelrhodopsin- 2-assisted circuit mapping of long-range callosal projections. *Nat. Neurosci.* **10**, 663 (2007).

97. L. Petreanu, T. Mao, S. M. Sternson, K. Svoboda, The subcellular organization of neocortical excitatory connections. *Nature* **457**, 1142 (2009).

98. H. Adesnik, M. Scanziani, Lateral competition for cortical space by layer-specific horizontal circuits. *Nature* **464**, 1155 (2010).

99. L. Galvani, De viribus electricitatis in motu musculari, commentarius. *Bonon Sci. Art Inst. Acad.* **7**, 364 (1791).

100. M. Scanziani, M. Häusser, Electrophysiology in the age of light. *Nature* **461**, 930 (2009).

101. D. H. Hubel, Tungsten microelectrodes for recording single units. *Science* **125**, 549 (1957).

102. G. Buzsáki, Large-scale recording of neuronal ensembles. *Nat. Neurosci.* 7, 446 (2004).

103. W. B. Scoville, B. Milner, Loss of recent memory after bilateral hippocampal lesions. *J. Neuro. Neurosurg. Psychiatry* **20**, 11 (1957).

104. G. Buzsáki, E. I. Moser, Memory, navigation and theta rhythm in the hippocampal-entorhinal system. *Nat. Neurosci.* **16**, 130 (2012).

105. L. M. Frank, E. N. Brown, M. A. Wilson, A comparison of the firing properties of putative excitatory and inhibitory neurons from CA1 and the entorhinal cortex. *J. Neurophysiol.* **86**, 2029 (2001).